SorLA and Amyloid Beta

Expression in Glioma

By

Morgan Huw Williams

A thesis submitted in partial fulfilment for the requirements

for the degree of MSc (by Research) at the University of

Central Lancashire

June 2019

STUDENT DECLARATION FORM

uclan
University of Central Lancashire

Type of Award   __Master of Science (by Research)_____

School   __Pharmacy & Biomedical Sciences _____

1.   **Concurrent registration for two or more academic awards**

I declare that while registered as a candidate for the research degree, I have not been a registered candidate or enrolled student for another award of the University or other academic or professional institution

2.   **Material submitted for another award**

I declare that no material contained in the thesis has been used in any other submission for an academic award and is solely my own work
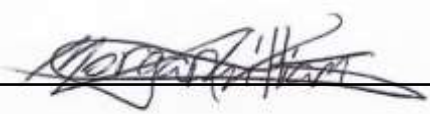
3.   **Collaboration**

Where a candidate's research programme is part of a collaborative project, the thesis must indicate in addition clearly the candidate's individual contribution and the extent of the collaboration. Please state below:

_____

4.   **Use of a Proof-reader**

No proof-reading service was used in the compilation of this thesis.

Signature of Candidate _____

Print name: __MORGAN HUW WILLIAMS _____

ACKNOWLEDGEMENTS

ABSTRACT

Glioma is the collective term for cancerous glial-cell tumours. The most prominent of these cancers is glioblastoma (GB); the most common primary malignant brain tumour and the most aggressive. Treatment options for GB are severely limited, not least because of an incomplete understanding of the molecular mechanisms underlying disease onset and progression.

SorLA is a widespread type 1 transmembrane protein involved as a sorting receptor for an array of ligands in multiple tissues. Most studies into SorLA have focused on its role in the pathological processing of amyloid precursor protein (APP) in Alzheimer's disease. Reduced SorLA expression increases amyloidogenic APP cleavage to liberate toxic forms of amyloid beta (Aβ). A few recent reports have linked enhanced SorLA expression to various malignancies including leukaemia, lymphoma, pancreatic and bile duct cancers. Ectodomain shedding of soluble SorLA (sSorLA) has been posited as a hypoxia-induced migration inducer, contributing to the malignancy. Indeed, it has been proposed that sSorLA may be a viable biomarker for these diseases.

SorLA's involvement in glioma has received very little attention. Using a combination of immunofluorescence (IF) imaging of GB cell lines *in vitro* and immunocytochemistry (IHC) of a mouse xenograft glioma model, this thesis tests the hypothesis that SorLA expression is upregulated in GB, and that Aβ is downregulated.

Analysis of IF confirmed expression of SorLA in GB cell lines and human foetal astrocytes. Differences in expression levels were not significant, likely owing to limitations of the methodology employed.

Standard histochemical analysis confirmed the success of the mouse xenograft model of GB in forming tumours. IHC using antibodies against SorLA in this model revealed staining in both tumour and non-tumour regions. Within the tumour itself, staining was restricted to

large extracellular deposits of significantly larger size than in non-tumour regions. Interestingly, the total SorLA staining was comparatively greater in non-tumour areas, where a more uniform pattern of intracellular staining was seen. Since the antibody employed could not distinguish between transmembrane and soluble forms of SorLA, due to the region of binding being found on both forms of the protein; this might indicate a propensity for sSorLA to be shed extracellularly within the tumour but remain intracellular in normal brain. Given the role of SorLA in Aβ production and the plaque-like structures seen within the tumours, IHC was performed to identify the presence of Aβ in tumour and non-tumour tissues. Aβ immunoreactivity was detected throughout the brain but localised to thread-like structures between cells and large extracellular plaques which resembled the senile plaques seen AD but did not co-localise with SorLA. Unexpectedly, a halo region of Aβ peripheral to the tumour was visible, with staining intensity decreasing with distance from the tumour margin. Whether this expression was an exfiltration of Aβ from the tumour or emanated from the tumour microenvironment was not an aim of this thesis, but would warrant further investigation.

In conclusion, this investigation revealed that SorLA is expressed in astrocytes and in glioma cell lines. Moreover, SorLA was expressed in a mouse glioma xenograft model and formed extracellular plaques within the tumour, most likely comprised of aggregations of sSorLA. This is due to sSorLA lacking the cytosolic tail motif unlike SorLA, which is kept membrane-bound by said motif. The study also found that amyloid beta was also present in tumour tissue in the form of extracellular plaques and in non-tumour tissue immediately peripheral to the tumour. Taken together, these data indicate that SorLA and Aβ may have a role in glioma and warrant further investigation, particularly as literature mentions that a lack of intracellular SorLA increases the presence of Aβ.

TABLE OF CONTENTS

LIST OF FIGURES

LIST OF TABLES

LIST OF APPENDICES

LIST OF ABBREVATIONS

1321N1	Human Brain Astrocytoma Cell Line
°C	Degrees Celsius
A555	Alexa Fluor 555
Ab	Antibody
AD	Alzheimer's Disease
AF	Alexa Fluor
APP	Amyloid Precursor Protein
BCA	Bicinchoninic Assay
BSA	Bovine Serum Albumin
BTNW	Brain Tumour Northwest
CNS	Central Nervous System
CSC	Cancer Stem-Like Cells
DAB	3,3'-Diaminobenzidine
DAPI	4' 6-diamidino-2-phenylindole
dH$_2$O	De-ionised Water
ECACC	European Collection of Authenticated Cell Cultures
ELISA	Enzyme-Linked Immunosorbent Assay
FACS	Fluorescence-Activated Cell Sorting
FBS	Foetal Bovine Serum
FOV	Field of View
GB	Glioblastoma multiforme
GFAP	Glial Fibrillary Acidic Protein
GFP	Green Fluorescent Protein
H&E	Harris' Haematoxylin, and Eosin
HSA	Human Serum Albumin
HSV1	Herpes Simplex Virus 1
HRP	Horseradish Peroxidase
IDH	Isocitrate Dehydrogenase
IF	Immunofluorescence
IHC	Immunohistochemistry
IMS	Industrial Methylated Spirit
LDL	Low-Density Lipoprotein
LDLR	Low-Density Lipoprotein Receptor
L	Litre
LRAD	LDL Receptor Class A Domain Containing 3

LRP	Lipoprotein Receptor Protein
NHA	Normal Human Astrocytes
NSC	Neural Stem Cell
NP	Nanoparticle
PBS	Phosphate Buffered Saline
RT	Room Temperature
SEM	Standard Error of the Mean
SorLA/SORL1/LR11	Sorting-Related Receptor With A-Type Repeats
sSorLA	Soluble Sorting-Related Receptor With A-Type Repeats
SVGp12	Human Foetus First-Trimester, Astroglia Cell Line
T98G	Male Human Glioblastoma Multiforme Cell Line
TACE	Tumour Necrosis Factor Alpha-Converting Enzyme
TBST	Tris-Buffered Saline and Tween 20
TMZ	Temozolomide
U87MG	Uppsala 87 Malignant Glioma Cell Line
UCLan	University of Central Lancashire
VLDLR	Very Low-Density Lipoprotein Receptor
VPS10	Vacuolar Protein Sorting 10
WB	Western Blot
WHO	World Health Organisation

CHAPTER 1

INTRODUCTION

1.1.   Glioma

Glioma is a wide-ranging term for cancerous tumours of a glial-cell origin. However, it is purported that glioma may arise from not just glial-cells but also neural stem cells (NSCs), these were found to be most likely to be susceptible to oncogenic mutations. These NSCs are the primary progenitor which can differentiate into glia (Zong *et al.,* 2015). Histologically, glioma can be classified into two types: circumscribed and diffuse. Examples of circumscribed glioma are; Juvenile Pilocytic Astrocytoma, Pleomorphic Xanthoastrocytoma and Subependymal Giant Cell Astrocytoma; which are known to not be aggressive and show clear differentiation between cancerous and healthy tissue. They are also able to be surgically resected with multimodal treatment having higher rates of success. Diffuse glioma, such as glioblastoma (GB), astrocytic, and oligodendroglial, is exceedingly difficult to curatively resect, this is due to their propensity to infiltrate other cell layers (Louis *et al.,* 2016).

GB is the most common of the primary malignant brain tumours and is the most aggressive with 45% of all primary brain and CNS tumours, as well as 81% of primary malignant brain tumours (McCarthy, 2011; Chen *et al.,* 2012; Ostrom *et al.,* 2014; Vogel *et al.,* 2017) are glioblastoma (GB). Grading of primary gliomas may be achieved using histological and, most recently, molecular markers from resected samples, which indicate the tumour's malignancy and invasiveness (Figure 1.1).

One such molecular marker ubiquitous amongst glioma is the isocitrate dehydrogenase (*IDH*) mutation. With *IDH1* mutations being identified in around 12% of gliomas studied by Parsons *et al.* (2008), with further studies identifying further *IDH1* and *IDH2* mutations in lower WHO grade glioma (Tateishi and Yamamoto, 2019). The *IDH*-mutant gliomas in the 2015 WHO grading is mainly associated with secondary gliomas, occurring in 10% of glioma patients (Louis *et al.,* 2016). However, the *IDH1* mutation largely confers a degree of more favourable prognosis in glioma depending upon further genetic mutations alongside the mutant as they tend to be less invasive (Price *et al.,* 2017).

The updated WHO grading of glioma defines GB as a grade IV tumour; indicating high malignancy, necrosis and infiltration of surrounding tissue (Ostrom *et al.,* 2014). In terms of GB aetiology, >90% of cases occur de novo, arising spontaneously within the glial tissue of the CNS. The remainder of GB are attributed to the malignant development of lower WHO-grade gliomas (Price & Chiocca, 2014).

WHO grades of select CNS tumours

Diffuse astrocytic and oligodendroglial tumours
Diffuse astrocytoma, IDH-mutant	II
Anaplastic astrocytoma, IDH-mutant	III
Glioblastoma, IDH-wildtype	IV
Glioblastoma, IDH-mutant	IV
Diffuse midline glioma, H3 K27M–mutant	IV
Oligodendroglioma, IDH-mutant and 1p/19q-codeleted	II
Anaplastic oligodendroglioma, IDH-mutant and 1p/19q-codeleted	III

Other astrocytic tumours
Pilocytic astrocytoma	I
Subependymal giant cell astrocytoma	I
Pleomorphic xanthoastrocytoma	II
Anaplastic pleomorphic xanthoastrocytoma	III

Figure 1.1. WHO 2016 classification of glioma tumours (Louis et al., 2016).

1.1.1. Diagnosis and treatment of glioma

GB previously glioblastoma multiforme – a reference to its diverse histological presentation, which is now known to extend to its heterogenous molecular presentation also (Gokden, 2017). This tumour heterogeneity combined with the diffuse nature of GB can make accurate classification challenging and means survival rates for patients are bleak. With the average survival, utilising current multimodal treatment of surgery, radiotherapy, and combined chemotherapy with Temozolomide (TMZ), being 20.2 months from identification, increasing from 14.6 months in 2005 (Stupp *et al.,* 2005; Tamimi & Malik, 2017; Kazda *et al.,* 2018). Surgery is only a temporary solution for most patients, however, as there is a 90% recurrence within 2 cm of the primary tumour area, known to be caused by residual neoplastic cells (Anghileri *et al.,* 2016; Hamard *et al.,* 2016). GB tumour heterogeneity (both intratumour and

intertumour) gives rise to new tumour cell subclones and hence poses significant challenges for developing new curative therapies; as treatments must be effective against all subclones (Anjum *et al.,* 2017). A further barrier to the development of effective diagnostic tools and therapies is an incomplete understanding of the molecular mechanisms governing tumour onset and progression. Hence, there is currently a pressing need to those identify molecules which are dysregulated in tumour and surrounding tissues which might, in turn, reveal new pathways to target.

1.2.   SorLA

Sorting-related receptor, L(DLR class) with A-type repeats (SorLA) is a 230kD mosaic type1 transmembrane protein conserved in humans (Willnow and Andersen, 2013). First identified in 1996, SorLA has been shown to be involved in cellular ligand transport and has been shown to be responsible for the regulation of amyloid precursor protein in Alzheimer's disease (AD; Eggert *et al.,* 2017). Recent evidence has linked SorLA expression to the development of several cancers, including biliary tract cancer, pancreatic cancer, and diffuse large B-cell lymphoma (McCarthy *et al.*, 2010; Terai *et al.,* 2016; Sugita *et al.,* 2016). This is through SorLA being upregulated, producing its soluble variant sSorLA at a higher rate, which the studies have indicated sSorLA as being a cell migrator. However, whether it has any role in GB remains unknown.

1.2.1.   SorLA Structure and distribution

SorLA's quaternary structure (Figure 1.2. A) consists of a ~700 amino acid VPS10 domain. Which, in tandem with complement-type repeats, enables its increased ligand binding ability, than if it was solely of the VPS10 domain or LDL receptor families (Quistgaard *et al.,* 2009; Nakata *et al.,* 2011). Between these two areas is a β-propeller structure, which is involved in

pH-dependent ligand discharge when SorLA relocates to the acidic endosome (pH <5.5)

(Willnow & Andersen, 2013). Connected to the base of the complement-type repeats are six

fibronectin-type III domains. This whole extracellular structure (excluding the VPS10 domain)

has been found to be very similar to those on the LDL LRPs (Schmidt *et al.*, 2017). Upon

SorLA's cytoplasmic tail there are three binding motifs for cytosolic adaptors within its amino

acid sequence: FANSHY; acidic motif; the Golgi-localising, gamma-adaptin ear homology

domain; and the ARF-interacting protein (Figure 1.2. B).
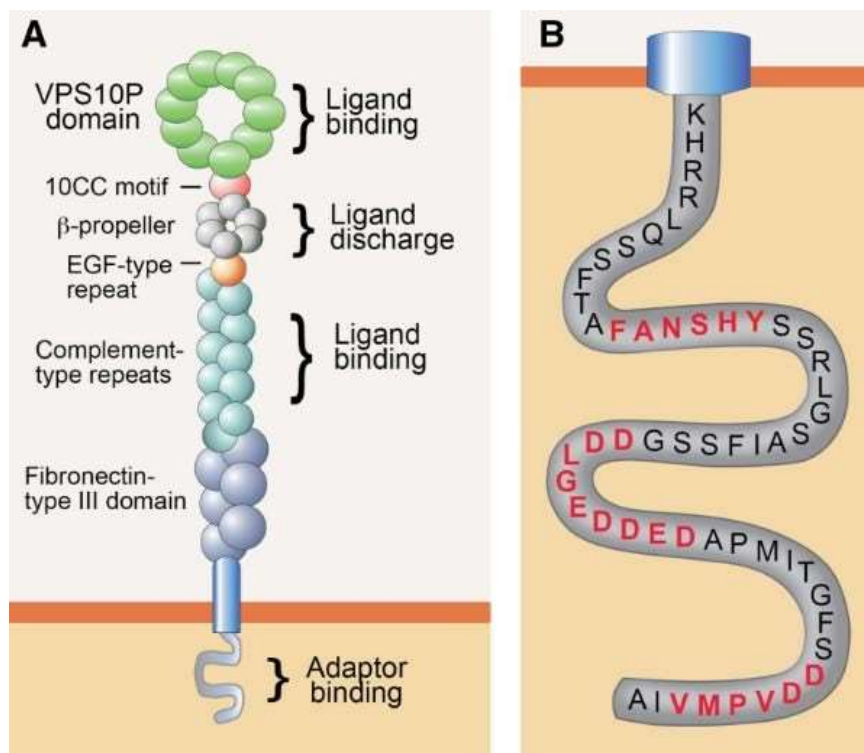
Figure 1.2. Structure of SorLA. A. Representation of SorLA's structure demonstrating the location of the known elements making up the protein and their functions. **B.** Focus on the 53 amino acid polypeptide chain comprising the cytosolic adaptor binding site, highlighting the three primary binding motifs (Adapted from Schmidt *et al.,* 2017).

SorLA plays a central role in the intracellular trafficking within various tissues, the most relevant to this research being neurones, glia, and the brain (Riedel *et al.,* 2002; Salgado *et al.,* 2013; Terai *et al.,* 2016; Schmidt & Willnow, 2016). SorLA is localised in cells primarily around the trans-Golgi and early endosome but is trafficked between both the secretory pathway and cell surface also. Acting as a sorting receptor, it uses its cytosolic adaptors to traffic various proteins and unrelated ligands (Hermey, 2009).

SorLA may also be released extracellularly. This soluble SorLA (sSorLA) is produced in several steps including cleavage of its cytoplasmic tail by the metalloprotease, TACE (Böhm *et al.,* 2006; Hermey, 2009). This ectodomain shedding liberates an almost-full length fragment (missing only the transmembrane portion) and appears to be low-level constitutive). It has been demonstrated that sSorLA release may be stimulated by extracellular factors and may have a role in interleukin-6 signaling (Hermey *et al.,* 2006; Larsen and Petersen, 2017). Moreover, altered sSorLA levels in biofluids have been detected in several disease states, including various cancers, meaning it is potentially non-specific, opening the possibility of its use as a diagnostic and prognostic marker (Ogita *et al.,* 2013; Fujimura *et al.,* 2014; Sugita *et al.,* 2016; Terai *et al.,* 2016).

1.3. SorLA in cancer

Dysregulated levels of SorLA have been identified in several cancers. SorLA has been specifically shown to be expressed on the cell membrane of leukaemic cells in acute leukaemia (AML and ALL) and serum levels of sSorLA were significantly increased (Sakai *et al.,* 2012). Enhanced serum sSorLA levels have also been reported in diffuse large B-cell lymphoma (Ohwada *et al.*, 2015), non-Hodgkin's lymphoma (Fujimara *et al.,* 2014)

The enhancement of SORL1 expression has also described in biliary tract and pancreatic cancer cells, with the patients' bile samples showing significantly increased levels of sSorLA

independent of cancer cells present (Terai *et al.,* 2016). Interestingly, the transcription levels of SORL1 were seen to be significantly elevated under hypoxic conditions, and during the peak of proliferation (Terai *et al.,* 2016).

There is currently limited published literature regarding SorLA's role in glioma. SorLA has been reported to be expressed throughout the nervous system and both murine C6 glioma and human astrocytoma cell line 1321N1 show appreciable SorLA expression (Salgado et al., 2012). In contrast to the data gathered in studies into other cancers, which might suggest that elevated SorLA tissue expression and sSorLA shedding may be a common feature of cancers, a reanalysis of microarray data from various astrocytomas by MacDonald and colleagues (2007) reported decreased levels of SORL1 mRNA in high-grade astrocytomas. While interesting, it should be noted that this study used data pooled from a mixture of paediatric and adult astrocytomas of varying classifications; moreover, transcript levels do not necessarily correlate well with cellular protein levels, which would be responsible for any cellular effect (Lui *et al.,* 2016).

1.4. SorLA in Alzheimer's disease

The clearest link between SorLA levels and human pathology is with Alzheimer's disease (AD), where increasing evidence links SorLA dysfunction or loss to increased risk (Schmidt *et al.,* 2017). AD is an incurable, progressive neurodegenerative disorder thought to be induced by an abnormal build-up of aggregated amyloid beta (Aβ) in and around brain cells, leading to declining cognition and death (National Health Service, 2018; National Institute of Neurological Disorders and Stroke, 2018). Abnormal production, accumulation and extracellular deposition of Aβ, forming neurotoxic senile plaques, is one of the longest-standing hypotheses for the cause of AD's widespread neuronal death (Du *et al.,* 2018). It is suggested that the formation of a slightly elongated form of Aβ, Aβ42, is responsible for

neurotoxicity and induces intraneuronal tau protein neurofibrillary tangle build-up; this entire process is sometimes termed the amyloid cascade hypothesis (Hardy and Higgins, 1992).

Willnow and Andersen (2013) summarised how the current theory for the production of neurotoxic Aβ peptides is due to the dysregulated proteolytic breakdown of the amyloid precursor protein (APP) during its movement between the secretory compartments, cell surface, and endosomes.

1.4.1. Amyloid precursor protein and amyloid beta

APP is an integral type I transmembrane glycoprotein that has a primary amino acid structure 639-770 length depending upon isoform (Yoshikai *et al.,* 1990). Post-translational modifications of the APP polypeptide lead to the formation of the protein's 6-domain quaternary structure which consists of: cytoplasmic C-terminal domain, transmembrane domain, E2 domain, Kunitz protease inhibitor domain, and an E1 domain (Dawkins and Small, 2014).

While its exact physiological functions haven't yet been fully elucidated, some of the functions of APP are thought contribute to the pathways which stimulate neural stem cell (NSC) proliferation and differentiation, owing to processing of APP being analogous to that of Notch, a known regulator of NSC differentiation (Ables *et al.,* 2011). APP has also been shown to act as an agent of neuronal repair through interaction with cell-adhesion molecules (Dawkins and Small, 2014).

The most widely studied role of APP is as a precursor protein to Aβ. Post-processing, APP is trafficked to the cell surface before being moved into the endosomal-lysosomal pathway, this leads to APP being partially degraded via proteolytic processing from β-secretase. This cleavage results in many fragments, but it is the membrane-bound C-terminal fragment (C99) that is then cleaved by γ-secretase to produce Aβ. Even in healthy individuals the exact type of Aβ produced isn't consistent, primarily varying between the 40-amino acid Aβ40 (80-90%)

and the 42-amino acid Aβ42 subtypes (5-10%), with the remaining types being isoforms of 2-40 amino acids long (Murphy and LeVine, 2010). The build-up of both Aβ40 and Aβ42 isoforms has been reported to be a consequence of reduced ability to degrade Aβ. Since the Aβ42 peptide is significantly more fibrillogenic, it drives the production of insoluble neuritic plaques which in turn cause neurotoxicity, tau pathology and eventual neurodegeneration. Hence, alterations of the levels of Aβ42 or the ratio of Aβ40:Aβ42 are key drivers of AD pathology (Kamentani and Hasegawa, 2018).

While Aβ is highly conserved across vertebrate species relatively little of its biological function is known. Despite its pathological role in AD, studies have shown that a depletion of Aβ is counterproductive to an organism's health, which in turn, gives an insight to the likely physiological roles Aβ plays or contributes to. These putative roles are many and diverse with one being that Aβ serves an antimicrobial function, evidenced by studies showing other amyloid peptides acting in that capacity (Kagan *et al.,* 2012). This was due to their ability to form fibrils and create perforations in cell membranes which can induce autolysis, effective for countering intracellular pathogens, as well as Aβ actions lending to potentially neutrophilic action whereby Aβ aggregates halt microbial movement (Brothers *et al.,* 2018). Furthermore, Lukiw et al. (2010) demonstrated viricidal actions with Aβ42 preventing HSV1 infection of human neuroglia co-cultures to the same degree as the anti-viral drug acyclovir.

Brothers et al. (2018) summarise further functions of Aβ as likely having roles in tumour suppression, rapid-response to blood-brain barrier leakage and regulating glutamatergic and cholinergic synapses.

Regarding tumour suppression, Aβ has been suggested to inhibit tumour growth when injected into human glioblastoma xenografts (Paris *et al.,* 2004). This work is further expanded upon where Aβ was shown to be able to inhibit the formation/growth of capillaries and at high enough concentrations, degrade them (Paris *et al.,* 2010). It is suggested in a review paper that this is linked to the affinity Aβ has for free metal ions, preventing their use by the tumour

(Brothers *et al.,* 2018). This is important as neovascularisation in glioma is crucial to its rapid growth and malignancy.

There has been little dedicated research to the role Aβ may play in glioma, with what few studies there are suggesting that Aβ can inhibit tumour growth, being shown to do this when injected into human glioblastoma xenografts (Paris *et al.,* 2004). Furthermore, Aβ was shown to be able to inhibit the formation/growth of capillaries and at high enough concentrations, degrade them (Paris et al., 2010). It is suggested in a review paper that this is linked to the affinity Aβ has for free metal ions, preventing their use by the tumour (Brothers *et al.,* 2018). This is important as neovascularisation in glioma is crucial to its rapid growth and malignancy.

1.4.2. SorLA protects against AD

Normal levels of SorLA are thought to protect against AD in a number of ways. Under normal conditions, SorLA colocalises with APP via its cytoplasmic and luminal domains, recycling it away from the endosome, reducing the amyloidogenic processing of APP to Aβ (Spoelgen *et al.,* 2006). SorLA is also thought to have a role in Aβ degradation, binding to and tagging monomeric Aβ for lysosomal degradation (Eggert *et al.,* 2017). Furthermore, SorLA is involved in disrupting the action of β-site APP-cleaving enzyme-1 (BACE1), another enzyme involved in the amyloidogenic processing of APP (Spoelgen *et al.,* 2006).

Several studies *in vitro* and in knockout mice have shown that the reduction or removal of SorLA increases Aβ production and conversely overexpression prevents production (reviewed in Schmidt *et al.,* 2017). Genetic studies into AD patients showed that there are identifiable SORL1 variants that confer risk for AD seemingly associated with inefficient SORL1 transcription/translation (Andersen *et al.,* 2016)

1.5.   The role of amyloid beta in glioma

A limited number of studies have suggested that Aβ may act to inhibit tumour growth. For example, injection of Aβ into human glioblastoma xenografts in mice inhibits angiogenesis and hence tumour growth (Paris *et al.,* 2004, 2010). This is important as neovascularisation in glioma is crucial to its rapid growth and malignancy. Notwithstanding, *in vitro* Aβ application to cancer cell lines, including the U87-L human glioblastoma cell line, also inhibited cell proliferation in a dose-dependent manner (Zhao *et al.,* 2009). The mechanisms behind this direct cellular inhibition are not known, although Aβ scavenging of free metal ions, limiting their availability to growing tumour cells has been suggested (Brothers *et al.,* 2018).

Given the accumulating evidence of a role for SorLA in various cancers, its expression in the brain and its role in producing Aβ, which has been demonstrated to inhibit tumour growth in glioblastoma models, investigation of a role for SorLA in glioblastoma is warranted.

1.6. Hypothesis

Based on the above, the hypothesis of this thesis is that:

Intracellular SorLA expression is enhanced and consequently Aβ expression is reduced in glioblastoma tissues.

1.7. Aims of the thesis

The specific aims of this thesis are:

1. To compare SorLA expression levels in human glioma cell lines to normal human astrocytes using western blotting and immunofluorescence.

2. To establish any morphological characteristics of SorLA subcellular distribution in glioma cell lines versus normal human astrocytes via immunofluorescence microscopy.

3. To investigate the expression of SorLA in a murine xenograft glioma model and quantify the expression of SorLA in tumour vs non-tumour brain regions.

4. To determine whether Aβ is detectable and/or altered in a murine xenograft glioma model in tumour vs non-tumour brain regions.

CHAPTER 2

MATERIALS & METHODS

2.1. Reagents

All general laboratory reagents were purchased from Fisher Scientific (Loughborough, UK) unless otherwise stated and were reagent-grade or higher. Where not otherwise indicated, all solutions were made up with distilled water.

2.2. Cell culture

The cell lines utilised in this study for experimentation were the U87MG and T98G human glioblastoma cell lines (both ECACC, Porton Down, UK) and SVGp12 human foetal astrocyte cell line (all ATCC, Teddington, UK). All cell lines were cultured in Eagle's Minimum Essential Medium (LONZA, Slough, UK) supplemented with; 10% (w/v) foetal bovine serum, penicillin/streptomycin (10,000 U/mL), L-Glutamine (200mM), non-essential amino acids (1x) and sodium pyruvate (100mM) all purchased from Fisher Scientific.

Normal human astrocytes (NHA), officially foetal astrocytes, were procured from LONZA (Slough, UK) and cultured by Norah Ulzheimer (University of Central Lancashire) for a separate study. NHA were grown in DMEM-F12 medium supplemented with 10% FBS, Glutamine (2mM), and 1% penicillin/streptomycin all from Fisher Scientific, Loughborough, UK.

All cell culture work was carried out in a Class II microbiological safety cabinet and using appropriate aseptic technique. Cell lines were grown in T75 flasks (Nunc, Roskilde, Danmark) and passaged by a trypsinisation at 70-80% confluency. Cells were gently washed in phosphate buffered saline (PBS) solution before 1x trypsin-EDTA was added to the flask and returned to the incubator for 2 minutes. Flasks were agitated to free adhered cells and checked under a cell culture light microscope (Optika, Ponteranica, Italy) to confirm cells were free-floating. Trypsin activity was quenched by the addition of 20 ml medium to each flask before contents were transferred to a 50ml Falcon tube and centrifuged at 1000G for 5 minutes. The supernatant was discarded, and the pellet resuspended in an appropriate volume of medium.

2.2.1. Cell seeding

For immunofluoresence imaging, cells were grown on No. 1.5 glass coverslips (Scientific Laboratory Supplies, Nottingham UK). Prior to seeding cells, coverslips were sterilised in 70% IMS and washed in PBS were placed in each well of a 12-well plate (Nunc, Roskilde, Denmark). Cells were seeded 24 hours prior to use as per seeding ratios in Appendix 4. Unfortunately, seeding density as a number of cells per cm^2 is unable to be produced for these cell lines.

NHA were seeded separately by Ms Norah Ulzheimer at 10,000 cells per cm^2 in 24 well plates containing No 1.5 glass coverslips. Plates were gently agitated in a circular motion to disperse cells and returned to the incubator for 24 hours to grow before use.

2.3. Immunofluorescence staining

Culture medium was removed from the seeded plates and the coverslips carefully washed x3 with PBS making sure not to disturb the cells. 4% w/v formaldehyde in PBS was applied for 15 minutes before washing x3 with PBS. Formaldehyde activity was quenched in 0.1M glycine (diluted in PBS) for 10 minutes and washed x3 with PBS. The cells were permeabilised with 0.1% Triton X-100 (diluted in PBS) for 4 minutes and washed x3 again with PBS.

The coverslips were incubated for 1 hour in a 5% bovine serum albumin (BSA) in PBS blocking solution at 4°C, and washed x3 afterwards with PBS. General-purpose tissue was laid on the laboratory bench and saturated with dH_2O before parafilm applied on top. 50 µL drops of mouse monoclonal anti-SorLA IgG primary antibody (3B6B11; Fisher Scientific, Loughbrough, UK) diluted 1:200 in PBS were added to the parafilm, and coverslips placed cell-side down onto the antibody drop, incubating for 30 minutes at room temperature. Control coverslips were treated with 50 µl blocking solution only in the same manner. Post-incubation coverslips were transferred back to the plate, washed x3 with PBS, before incubation for 30 minutes with Alexa Fluor 555 (A555) goat anti-mouse secondary antibody diluted 1:200 in PBS (Fisher

Scientific, Loughbrough, UK). After washing to remove unbound secondary antibody, coverslips were mounted to Fisherbrand T/F ground microscope slides with ProLong Diamond antifade with DAPI (to label nuclei). They were left to cure at room temperature in the dark overnight; then sealed with nail polish and stored at 4°C in the dark until use.

2.4. Fluorescence Microscopy

The slides were removed from the 4°C fridge and left for 20 minutes to return to room temperature prior to imaging. Fluorescence was visualised using an Axio Observer.Z1 Inverted Microscope equipped with HXP 120 V illumination (set at 25% power for DAPI and 50% power for A555) and dsRed/DAPI filter sets. Images were acquired using x20 PL Apo (0.8 NA) and x40 PL Apo (1.2 NA) oil objectives, AxioCam MRm camera and integrated Zeiss Pro 2 Blue image-capture software (Carl Zeiss Limited, Cambridge, UK). Prior to image capture optimal exposure levels were determined, to create a setting which worked for all slides. For overview imaging and calculation of IF staining intensity, a x20 PL Apo (0.8 NA) objective and exposure times of 100ms for DAPI and 500ms for A555 were used. Single images were collected from five random separate fields of view at x20 magnification per coverslip, with three replicate coverslips produced for each cell line, for three separate experiments (n=3), giving a total of 9 replicates. For higher magnification subcellular imaging, a x40 PL Apo (1.2 NA) oil objective and exposure times of 250ms for DAPI and 580ms for A555 were employed. Representative images from n=3 experiments are shown.

2.4.1. Analysis of fluorescence intensity

ImageJ2 (Fiji, 2017) analysis software was utilised for analysis of the fluorescence images and calculation of relative fluorescence intensities. The fluorescence intensity for each whole image was measured and divided by the number of Alexa Fluor 555 positive cells present to determine the fluorescence intensity per cell for each field of view. The average background

fluorescence, calculated from three random acellular regions in each image, was then subtracted from the relevant image's fluorescence intensity. A mean Alexa Fluor 555 fluorescence value per cell (indicative of SorLA staining intensity) was then calculated for each cell type.

Shapiro-Wilk normality tests confirmed that all data were normally distributed. A p-value of 0.05 was considered significant. Fluorescence intensities between cell types were compared using post-hoc one-way analyses of variance (ANOVA) on GraphPad Prism 7.04 (GraphPad Software, La Jolla, USA). Associated graphs were compiled to better represent the data where appropriate.

2.5. Immunohistochemistry in mouse brain tissue

2.5.1. Mouse xenograft glioma model

Surgical stereotactic implantation of human U87MG glioma cells was performed by Ms Vicky Metcalf and Dr Chris Smith (University of Central Lancashire, UK). Mice (BALB/c homozygous, Charles River) weighing approximately 25g were anaesthetised with isoflurane in oxygen and mounted in a stereotactic frame (Kopf Instruments, Tujunga, USA) with anaesthesia maintained in a 50:50 isoflurane in oxygen:nitrous oxide mixture. The skin overlying the skull was sterilised and a midline incision made so that the sutures of bregma and lambda were visible when the skin was retracted. The bone 1 mm lateral and 1 mm anterior to bregma was thinned and approximately 40,000

U87MG cells in 2 μl sterile PBS were injected 3 mm below the surface of the skull into the striatum. The cell suspension was injected at a flow rate of 1 μl/min and the needle slowly withdrawn. The hole was sealed with bone wax and the skin closed with vet bond. The animals were administered Metacam (5mg/kg) and Flamazine applied liberally to the wound before recovering. When fully recovered, mice were returned to the IVC home cage with *ad libitum*

access to sterile chow and water. Mice were euthanised when clinical condition deteriorated, the brain was removed and fixed in 10% (w/v) formalin until use.

The animal experiments were done in full accordance with UK Animals (Scientific Procedures) Act 1086 and European Direct 2010/63/EU legislation. Work was performed under project licence 70/7938 New Strategies for the Diagnosis and Treatment of Glioma granted by UK Home Office following scrutiny by UCLAN Animal Welfare and Ethical Review Board.

2.5.2. Processing & embedding of mouse xenograft brains

Brains were cut into 2 mm coronal slices in a brain matrix and stored in 10% formalin before being processed and embedded by Royal Preston Hospital Pathology Lab. Sections were exposed to a series of graded ethanol solutions, xylene, formalin, and paraffin wax in a Leica PELORIS Rapid Tissue Processor (see Table 2.1 for method). The processed tissue was orientated to allow coronal sections be taken and embedded in paraffin wax.

Table 2.1 - Tissue processing protocol

REAGENT	TIME (MINS)	TEMPERATURE (°C)
FORMALIN	44	45
ETHANOL (30%)	30	45
ETHANOL (50%)	30	45
ETHANOL (70%)	30	45
ETHANOL (80%)	30	45
ETHANOL (95%)	30	45
ETHANOL (100%)	90	45
XYLENE	45	45
XYLENE	45	45
XYLENE	90	45
WAX	60	65
WAX	60	65
WAX	60	65

2.5.3. Immunohistochemistry reagents

Antibodies employed for immunohistochemistry (IHC) in this study are outlined in table 2.2. Avidin Biotin Complex HRP anti-mouse or anti-rabbit, and DAB (HRP) chromogen kits were purchased from Vector Labs, Peterborough, UK. Bovine serum albumin (BSA), citric acid (anhydrous), ethanol, glacial acetic acid, haematoxylin, hydrogen peroxide 30% (w/v), mercuric oxide, potassium alum, and Tween 20 were all purchased from Fisher Scientific, Loughborough, UK. Harris haematoxylin, citric acid buffer, and quenching solution preparation protocols can be found in Appendix 1, 2, 3 respectively.

Table 2.2 - Antibodies

ANTIBODY	ISOTYPE	MONO/POLYCLONAL	SOURCE	DILUTION
ANTI-SORLA (AB190684)	Rabbit	Monoclonal	Abcam, Cambridge, USA	1:250 (IHC)
ANTI-GFAP (G9269)	Rabbit	Polyclonal	Sigma-Aldrich, Dorset, UK	1:500 (IHC)
ANTI-B-AMYLOID (6E10)	Mouse	Monoclonal	BioLegend, London, UK	1:500 (IHC)
ANTI-RABBIT BIOTINYLATED (PK-6101)	Goat	/	Vector Laboratories, Peterborough, UK	1:200 (IHC)
ANTI-MOUSE BIOTINYLATED (PK-6102)	Rabbit	/	Vector Laboratories, Peterborough, UK	1:200 (IHC)
IgG isotype control	Rabbit	/	Fisher Scientific, Loughborough, UK	1:250 (IHC)

2.5.4. Immunohistochemical staining of mouse xenograft brain sections

Mouse tissue blocks were cooled on ice before 4μm sections were cut on a microtome (Thermoscientific Microm HM-325) and mounted on slides (SuperFrost Plus, ThermoScientific) before being baked at 60°C for 1 hour.

Each brain was subjected to five staining treatments; anti-SorLA with haematoxylin counterstain, anti-SorLA without counterstain, anti-β-Amyloid, anti-GFAP as a positive control, and IgG isotype control. Immunolabelling for each treatment was repeated three times for each brain.

Sections were dewaxed and dehydrated in xylene for 5 minutes twice and ethanol for 5 minutes twice before exposed to citric acid (pH 6.0 w/ 0.75ml Tween 20) at 95 °C for 20 minutes (Dako PT Link) for antigen retrieval. Sections were transferred and submerged in tap water for 5 minutes before endogenous peroxidase activity was quenched by 0.3 % hydrogen peroxide solution in methanol for 15 minutes.

Non-specific binding was blocked using either an anti-rabbit or anti-mouse blocking serum, as appropriate, for 30 minutes (Vectorstain Elite ABC kit, Vector Laboratories, UK), with excess serum washed off using PBS. Primary antibody against SorLA, GFAP or β-Amyloid, or isotype control (see Table 2.2) was applied for 1 hour before sections were washed once with PBS and incubated for 30 minutes with the biotinylated secondary antibody.

The slides were washed with PBS before VECTASTAIN *Elite* ABC reagent was applied for 30 minutes. After another PBS wash, DAB peroxidase was applied for 2 minutes. The sections were washed with dH$_2$O before counterstaining, where needed, in Harris haematoxylin for 5 minutes. Counterstained sections were left under running tap water for 5 minutes before washing in an acid-alcohol solution for 45 seconds and rinsed with Scott's Tap Water. All

sections were dehydrated in 95 % ethanol for 10 dips, twice-over, and cleared in xylene for the same. Slides were mounted and coverslipped using DPX mountant.

2.5.5. IHC image capture and analysis

A Nikon Eclipse E200 microscope fitted with a CMEX DC.5000 camera was used to take x4 and x40 images of sections and visualised on a PC running ImageFocus V3.0 imaging software (Nikon UK Limited, Kingston Upon Thames, UK). Individual section images taken at x4 were stitched together image formatting tools in Microsoft Word 2016 to create a composite image of the whole brain section.

ImageJ2 (Fiji, 2017) analysis software was utilised for the analysis of staining densities for all IHC images. Prior to colour deconvolution in haematoxylin-DAB (HDAB) channels, the RGB values were determined in the empty areas of the slide and if not within 5 % of 255 on the grayscale "Process – Subtract background" was used. The "colour deconvolution" plugin was utilised according to HDAB profile, separating the image according to haematoxylin-only, DAB-only, and background. The DAB-only image was termed in the software as "colour 2" and was selected; whereby the image had its area (μm^2) and mean grey value (intensity) measured. The value of intensity was determined by the formula given by Fuhrich $et\ al.$: $f = 255 - i$, where $f =$ final DAB intensity, $i =$ mean DAB intensity obtained from the software; i ranges from 0 (zero = dark brown/black), to 255 (totally white).

Three regions of interest within the tumour and three outside the tumour from each slide were analysed for each section. Cells were counted on the H&E stained images using the ImageJ counting tool and the average grey scale determined in similar regions of interest in the adjacent sections. The mean grey scale per cell or per area could therefore be reported.

Statistically significant differences in mean grey scale values between tumour and non-tumour were determined by a paired samples t-test using GraphPad Prism 7.04 (GraphPad Software, La Jolla, USA). A p-value of 0.05 was considered significant throughout.

CHAPTER 3

# RESULTS

3.1. Western blotting for SorLA expression *in vitro*

The first aim of this thesis was to determine relative SorLA expression in glioma cell lines compared to a foetal astrocyte cell line and primary normal human astrocytes. Cells were cultured and lysates prepared for western blotting (WB), however ongoing problems were encountered which made the WB approach unviable for this project. Prepared lysates were tested for other antibodies and for beta actin, yielding clean bands of expected size. However, despite multiple antibodies being trialed, staining for SorLA yielded no bands, smears and/or inconsistently-sized faint bands. These problems may alternatively have been due incomplete SorLA solubilisation in lysates, as SorLA is a transmembrane protein. Harsher solubilisation and denaturation approaches were tested, but findings remained inconsistent. Consequently, given the time-pressures of the project a semi-quantitative method of immunofluorescence staining, and image analysis was selected to investigate relative expression levels. This approach had provided an additional angle for analysis; to investigate any alterations in the sub-cellular distribution of SorLA between cancerous and non-cancerous cells.

3.2. Semi-quantitative analysis of SorLA expression by immunofluorescence

Human glioma cell lines (U87MG and T98G), a human foetal cell line (SVGp12) and normal human astrocytes (NHA (foetal astrocytes)) were fixed and immunostained for SorLA revealing fluorescence in all cell types (Figure 3.1, right-hand panel). To confirm the specificity of staining of the anti-SorLA antibody, negative control slides were prepared using BSA in place of the antibody (Figure 3.1, left-hand panel). Visualisation of these cells using the same settings as for the antibody-stained slides indicated only a minimum of background fluorescence, indicating that the clear fluorescence seen in the test slides was from specific binding of the primary antibody rather than from excessive autofluorescence or non-specific secondary antibody staining (Figure 3.1).
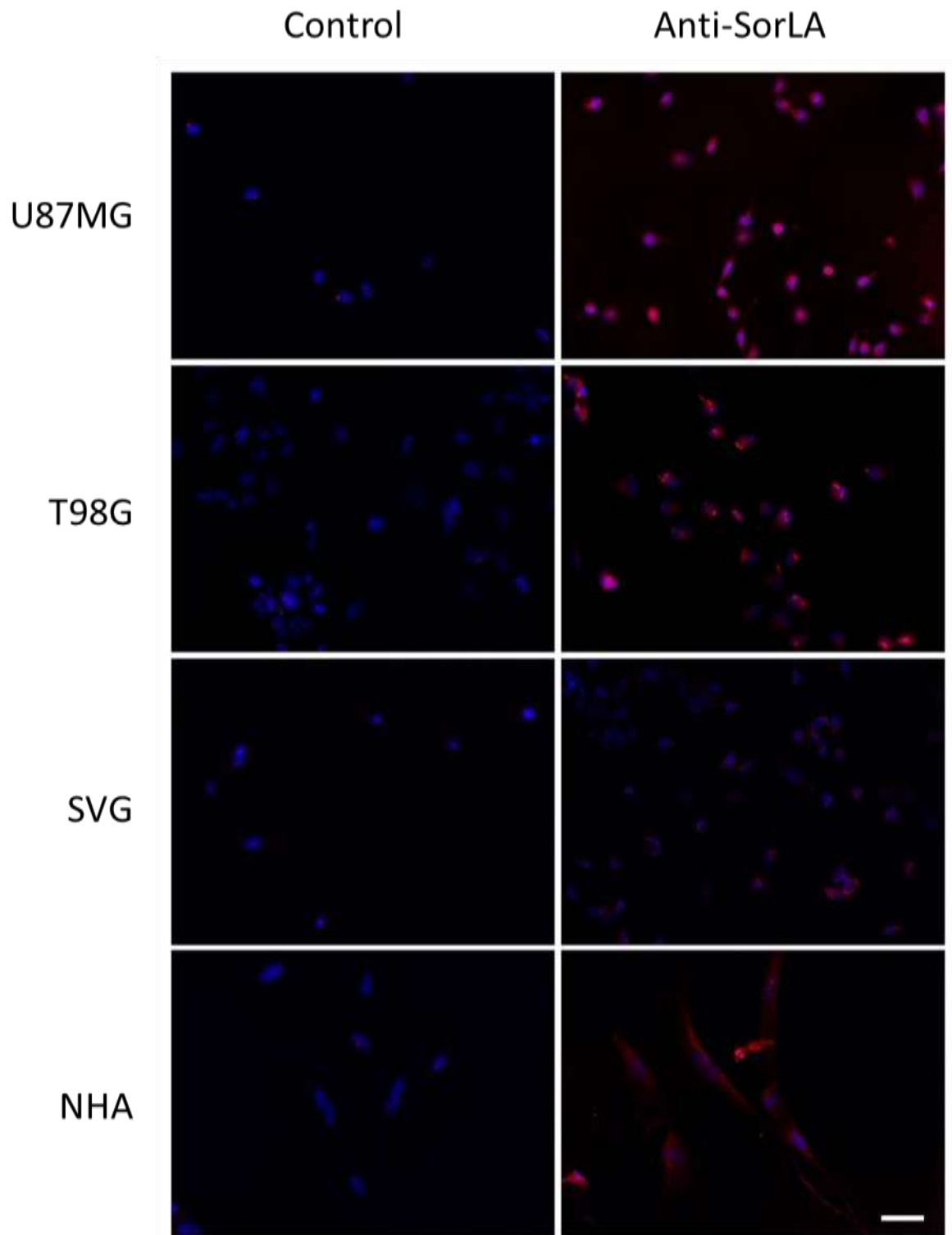
Figure 3.1. SorLA Expression in cell lines. Exemplar images, taken using fluorescence deconvolution microscopy, showing the immunoreactivity of SorLA (red) within the cell lines. For comparison, controls which replaced primary antibody with BSA-only are shown. DAPI stained nuclei, blue. Replicate data can be found in Appendix 14. Magnification x20, n=3, scale bar 50 μm.

In order to compare staining intensities as a semi-quantitative measure of SorLA expression levels, fluorescence images were collected from three separate staining preparations per cell line (five random fields of view per slide) at 20x magnification. These data were analysed using ImageJ. Following the subtraction of background fluorescence, a mean fluorescence level per cell for each cell type was calculated on a scale of 1 to 250 (Figure 3.2). Normal human astrocytes (NHA) revealed the highest level of fluorescence (mean grey scale intensity, M = 50.7, SEM = 14.4), while the foetal human astrocyte cell line, SVGp12, returned the lowest (mean grey scale intensity, M = 17.4, SEM = 2.4). The two glioma cell lines tested, U87MG and T98G, provided similar intensity values to one another (mean grey scale intensities, M = 30.2, SEM = 7.8 and M = 28.1, SEM = 13.7, respectively). A one-way ANOVA, however, revealed that there was no significant difference between any of the staining intensities of the four cell types ($F_{(4, 20)}$ = 1.966, p = 0.139).
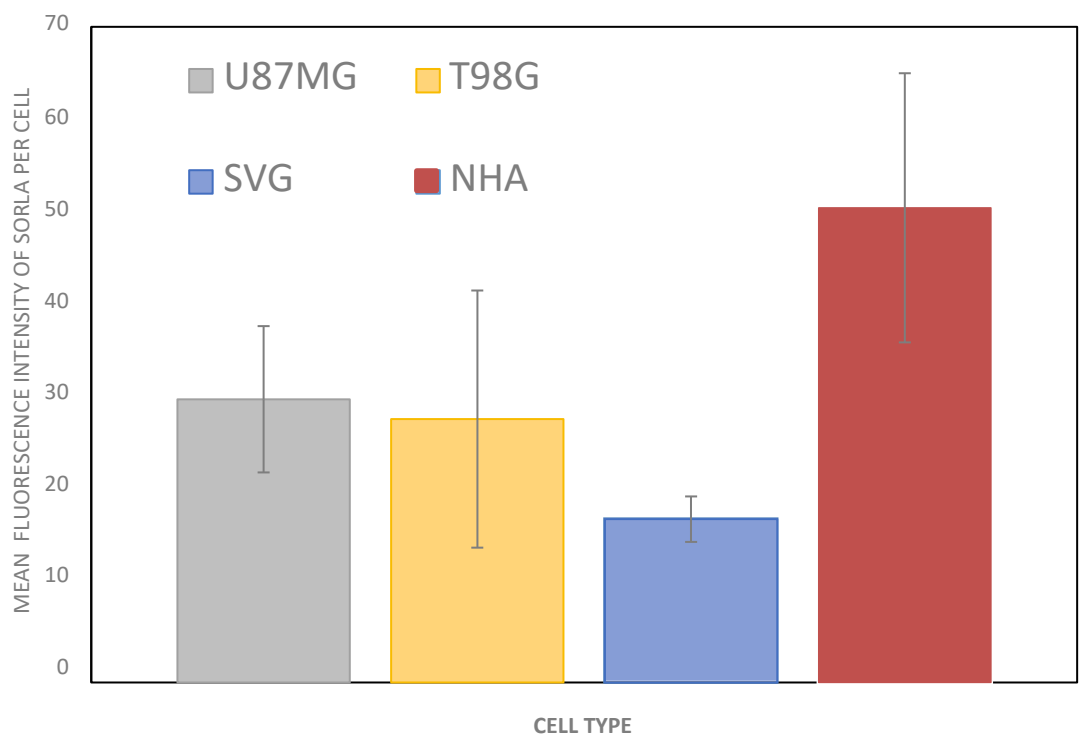
Figure 3.2. Fluorescence intensities between SorLA-stained glioma and non-glioma cells. U87MG and T98G glioma cell lines, SVG-p12 human foetal astrocytes and primary normal human astrocytes (NHA) were immunofluorescentally stained for SorLA. Mean fluorescence intensities per cell were calculated on a scale of 1-250. Tabulated data can be found in Appendix 8. *P* = ns, n=3 experiments, 5x FOV per experiment. Error bars = SEM.

3.3. Subcellular distribution of SorLA in glioma cell lines and non-cancerous cells

The role of SorLA as a sorting receptor depends upon its trafficking throughout endomembrane compartments within the cell, and to and from the cell membrane (Schmidt & Willnow, 2016). Glioma cell lines and the control cells exhibited a punctate staining pattern, consistent with SorLA localisation to intracellular membranes (Figure 3.3). Staining was also evident at the cell surface. Beyond the gross overall morphological differences between each cell type, the subcellular staining patterns within each cell type were indistinguishable from one another. In all cases the distribution pattern correlate with what would be expected in SorLA expressing cells based upon previously published studies (Gowrishkanar *et al.,* 2015).
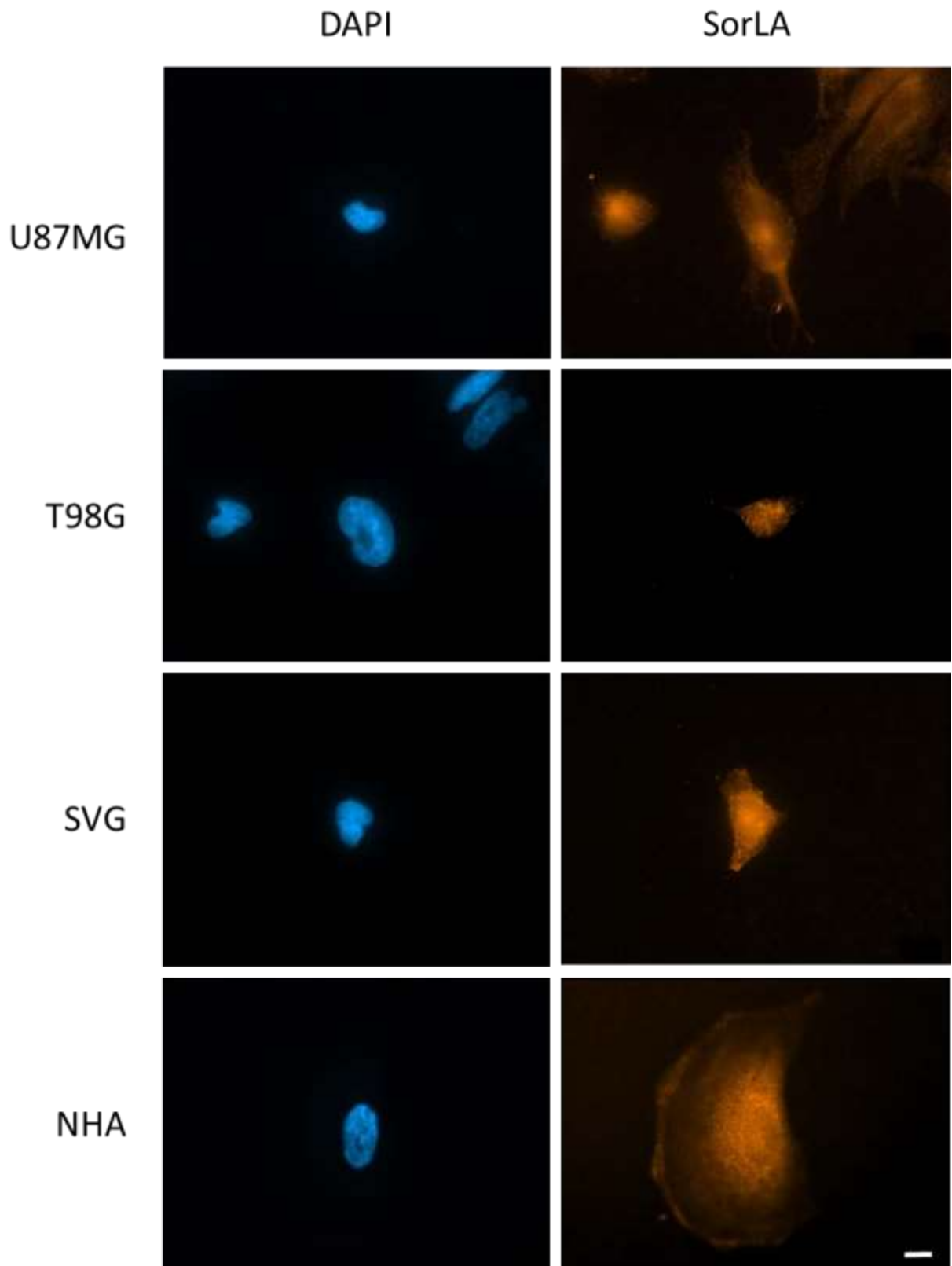
Figure 3.3. Subcellular distribution of SorLA across the cell lines. Exemplar images, taken using fluorescence deconvolution microscopy, showing similar patterns of intracellular staining. Magnification x65 'oil', n=3, scale bar 10µm.

3.4   Immunohistochemical localisation of SorLA in a mouse tumour xenograft model

3.4.1.   Preliminary validation of tumour and antibody optimisation

The presence of a tumour within the mouse brains A, B, and C, used in this study was confirmed following staining with haematoxylin & eosin. Haematoxylin selectively stained cell nuclei blue that contrasted with the pink/red of eosin. At low magnification a clearly encapsulated and demarcated tumour is evident in each brain (Figure 3.4). At higher magnification the smaller cells and hypercellularity is evident with an average cell density in the tumour of 0.63 ±0.01 cell/μm^2 compared to non-tumour regions with 0.22±0.01 cell/μm^2 (Appendix 5C).
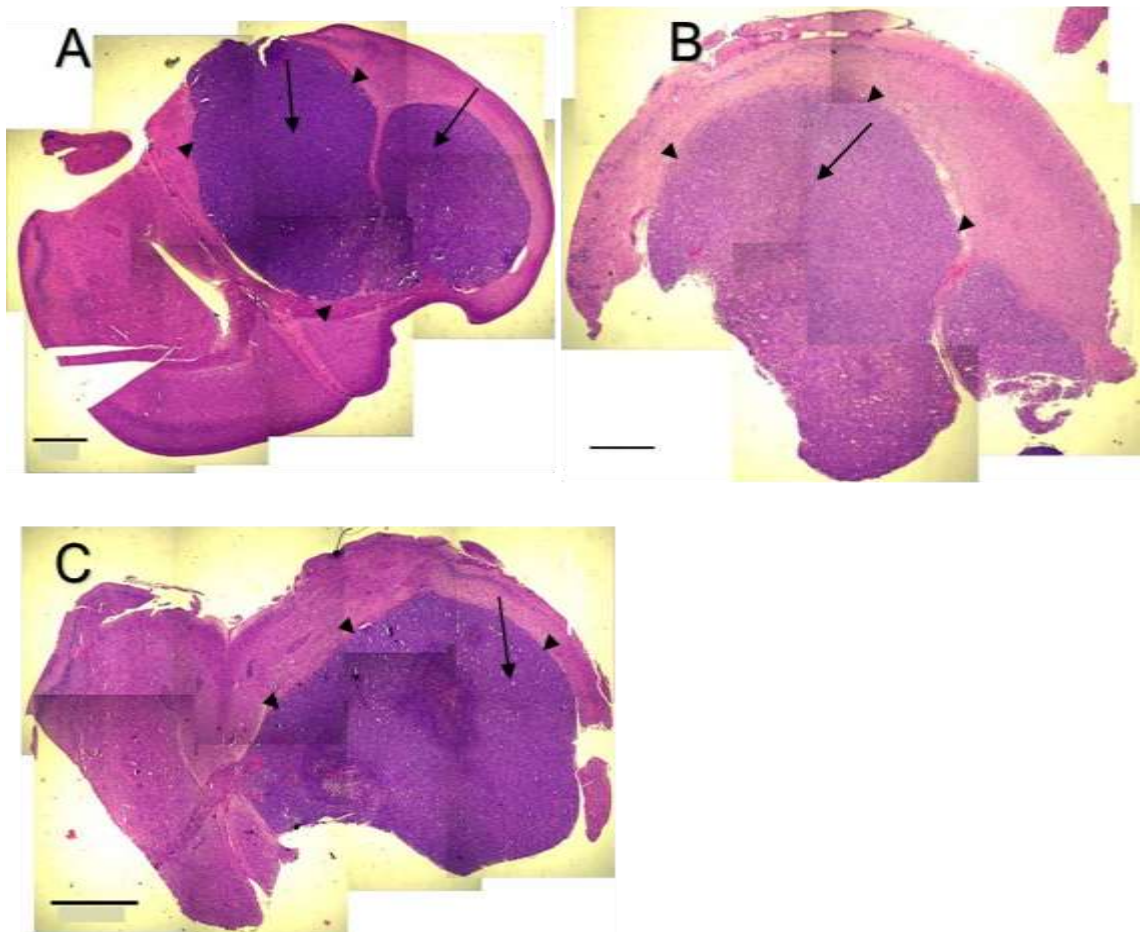
Figure 3.4. Haematoxylin & eosin stained murine xenograft U87MG models. Composite images showing tumours within the anterior region following U87MG xenograft. Tumour is evident by the hypercellularity (black arrows) and encapsulation of these areas (arrow heads) within the tissue. Scale bars A, C, 1 mm; B, 500 µm, n=3.

Antibodies were optimised in brain sections that lacked tumour. Immunoreactivity to the various antibodies were observed and a working concentration of 1:250 deemed appropriate for SorLA and 1:500 for Aβ (Appendix 9 and 10). In sections exposed to the IgG isotype negative control or when primary antibody was omitted no immunoreactivity was seen (Appendix 11).

3.4.2. SorLA expression in mouse tumour brain

Marked SorLA immunoreactivity was seen throughout the U87MG tumours from all three mice (Figure 3.5). Labelling was in dense plaques that ranged between approximately 10 μm^2 and 850 μm^2 and was significantly more prevalent than in non-tumour tissue when the area of SorLA plaques were compared (Figure 3.5 B, M = 0.268, SD = 0.149, SEM = 0.016); t(89) = 17.07, p<0.001). The large variation in area of SorLA plaques within the tumour, reflecting the wide range of plaque sizes. Light immunoreactivity was seen throughout the non-tumour tissue and brain contralateral to the tumour but with only infrequent SorLA positive plaques. In some sections, a region of lower immunostaining and haematoxylin staining was seen within the tumour. This may be due to needle damage or a necrotic core developing within the tumour (Figure 3.5, black arrows).

The greyscale intensity of SorLA confirmed quantitatively higher SorLA staining within the tumour as paired t-test analysis between the tumour and non- tumour regions demonstrated a highly significant difference in intensities (M = 64.98, SD = 44.18, SEM = 8.503); t(26) = 7.642, p<0.001) (Figure 3.6A).

At higher magnification and with haematoxylin counterstain the extracellular presence of SorLA plaques within the tumour are apparent (Figure 3.7, asterisks). In non-tumour regions most SorLA immunoreactivity is intracellular and associated with haemotoxylin (Figure 3.7, white arrows). This could be indicative of an alteration in SorLA ectodomain shedding, since the antibody utilised would recognise both transmembrane and shed soluble SorLA.

A

*

100 μm

B

*

100 μm

C

100 μm

D

E

F

100 μm
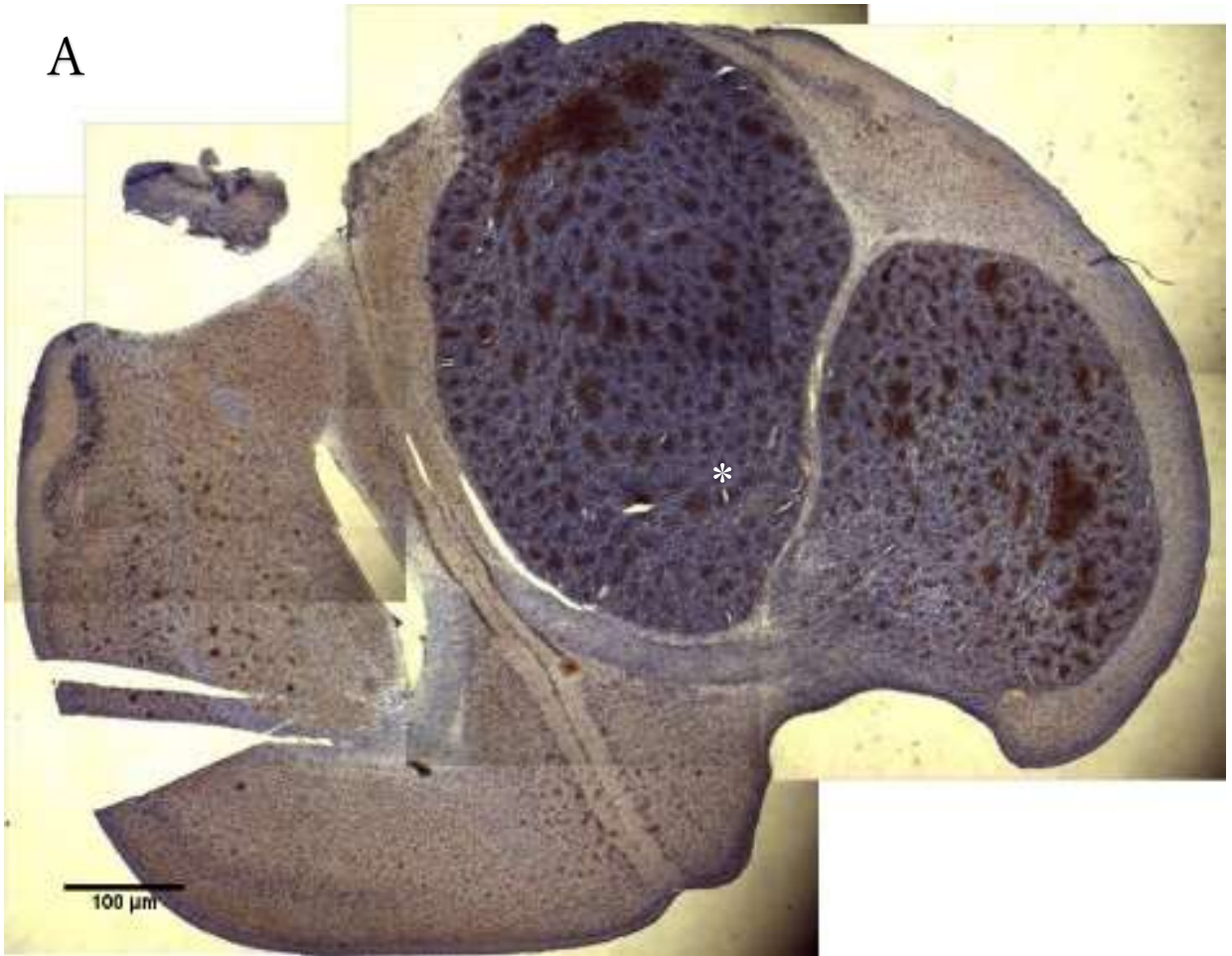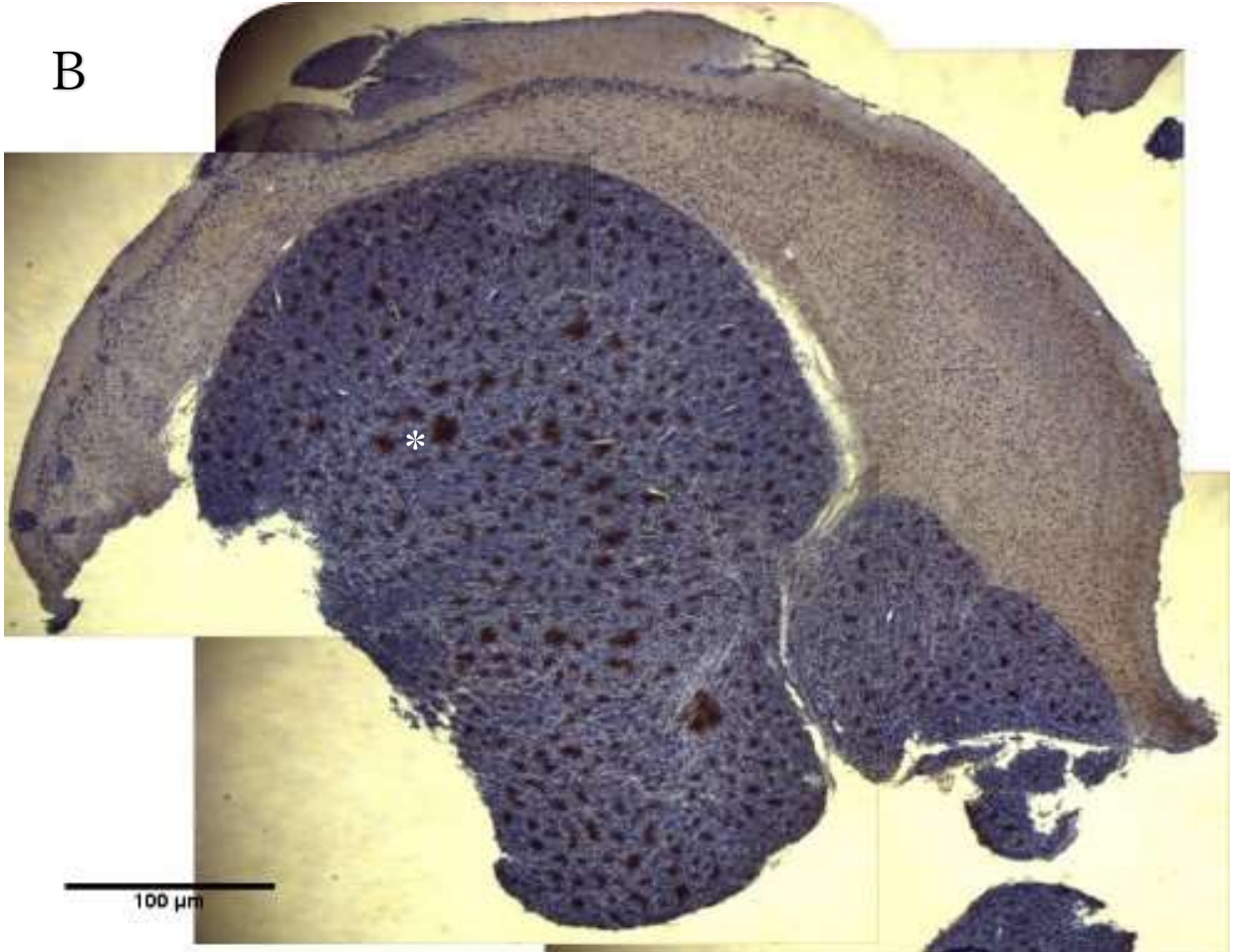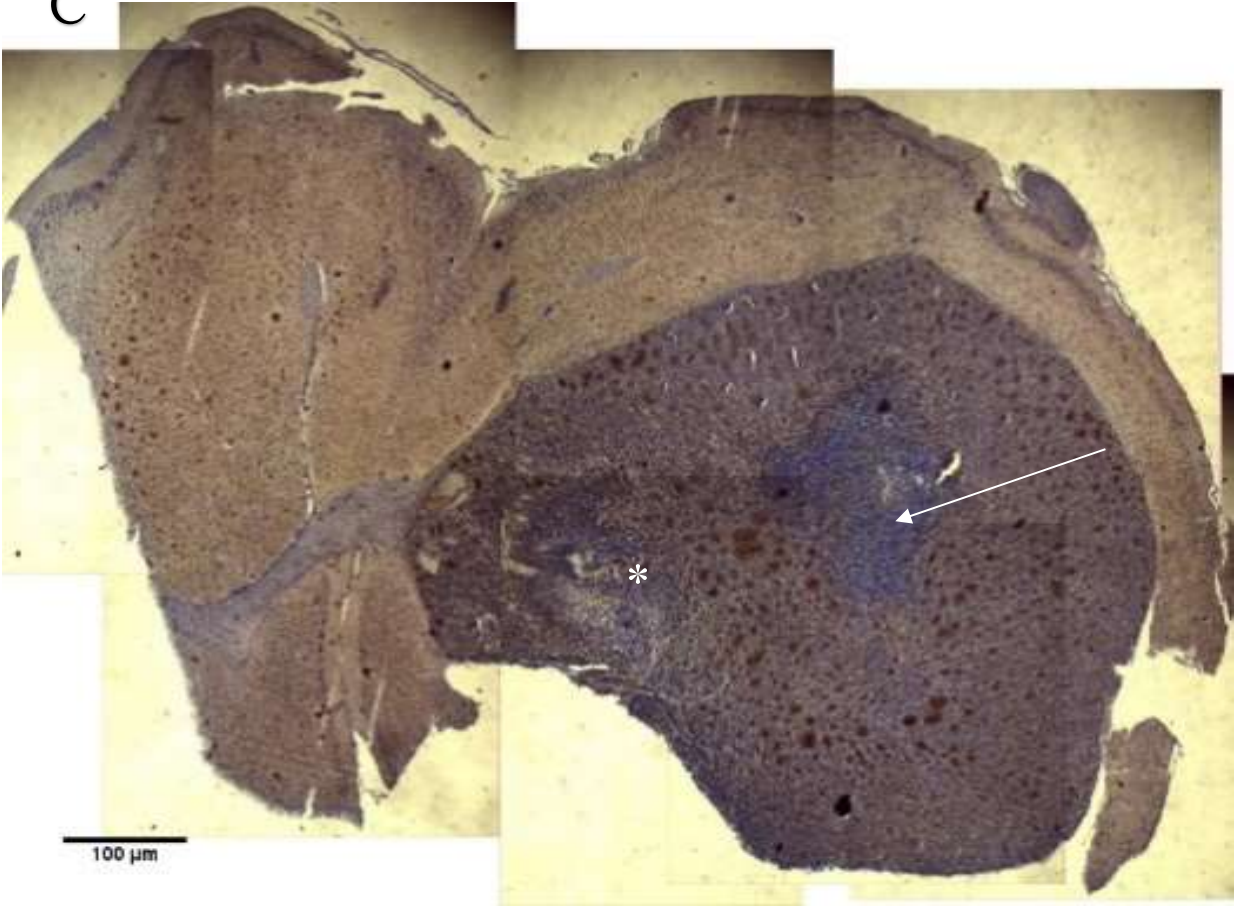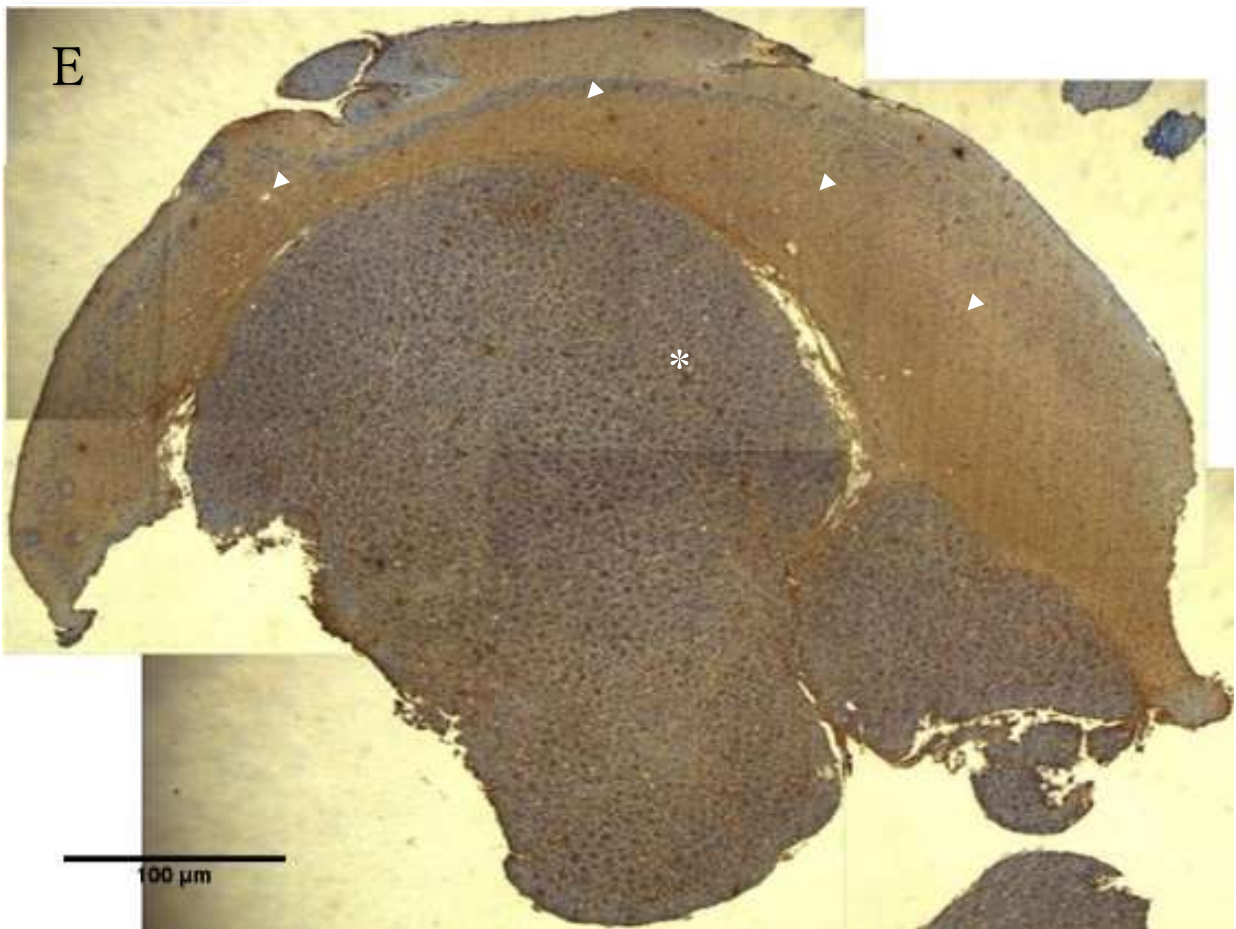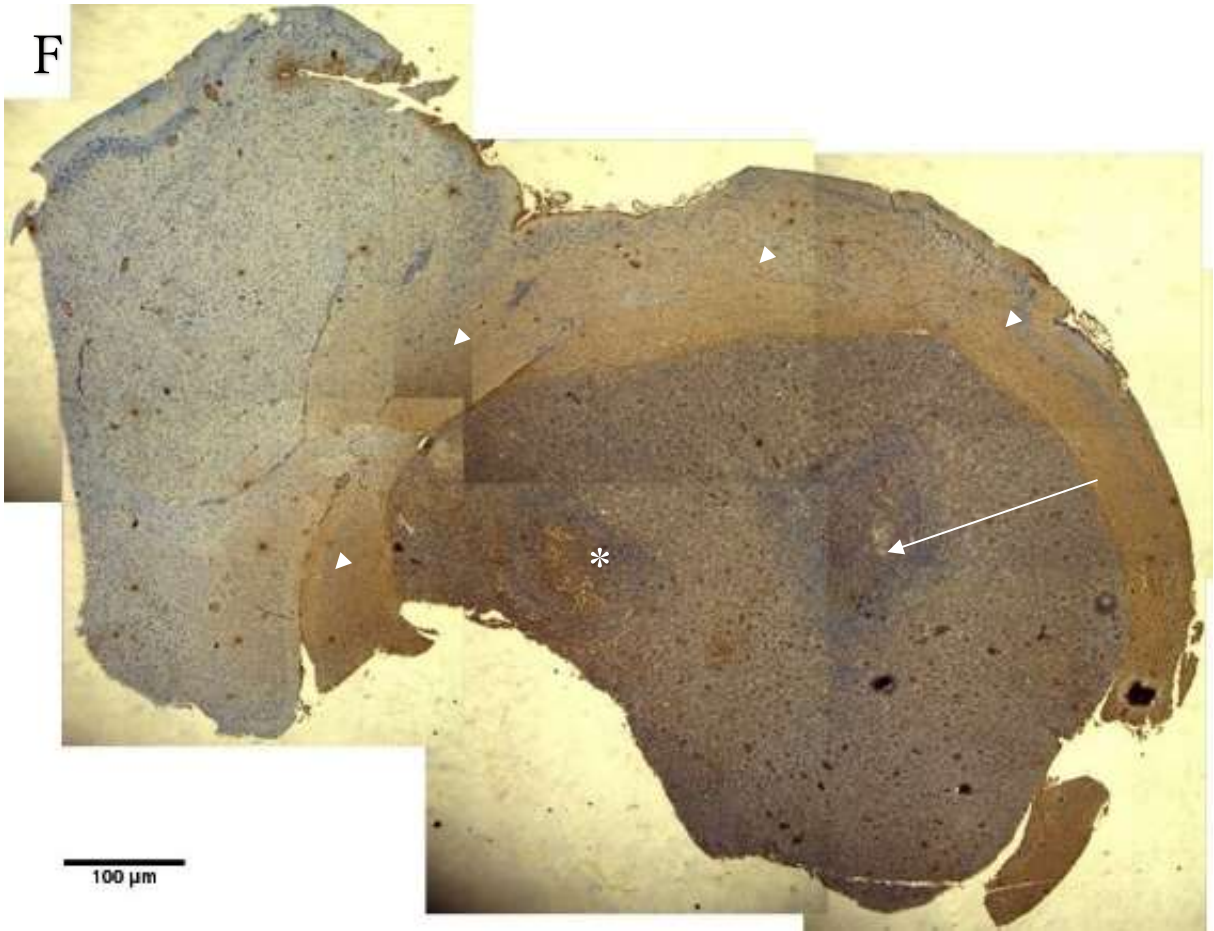
G
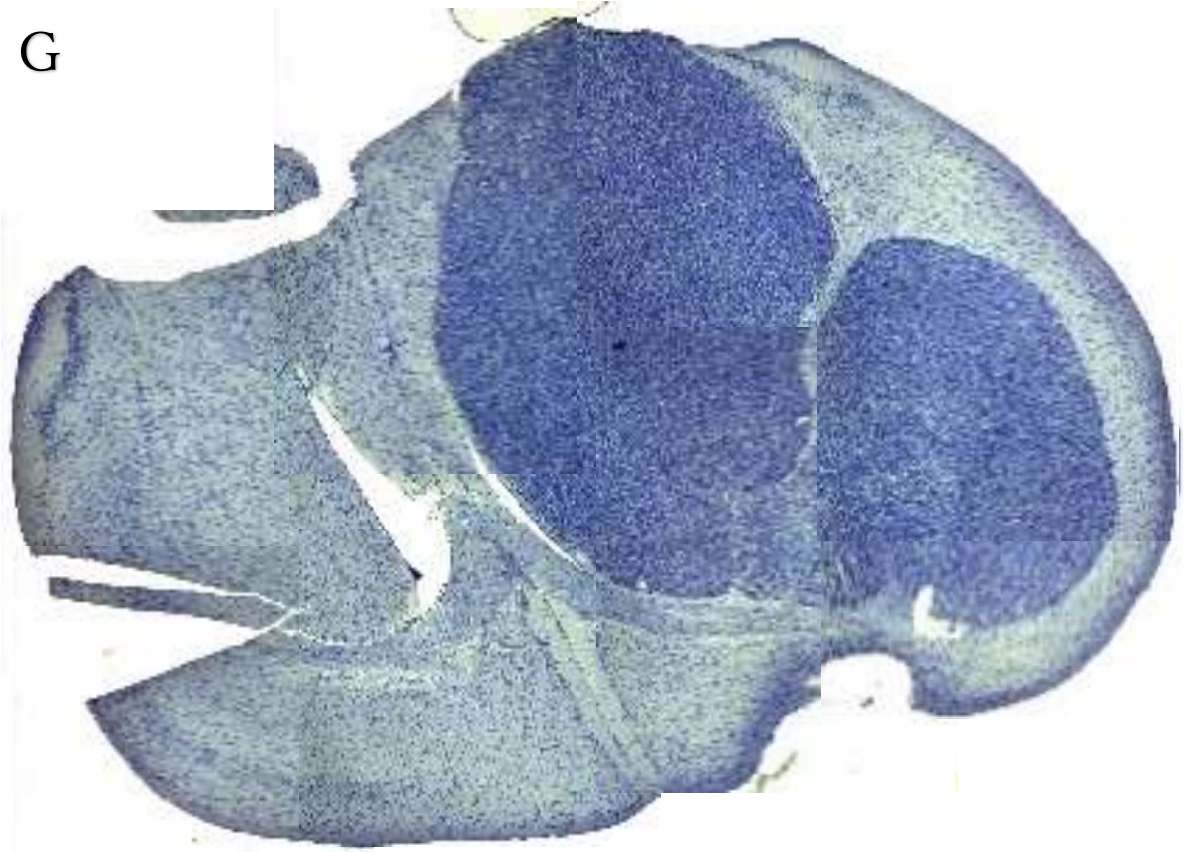
H
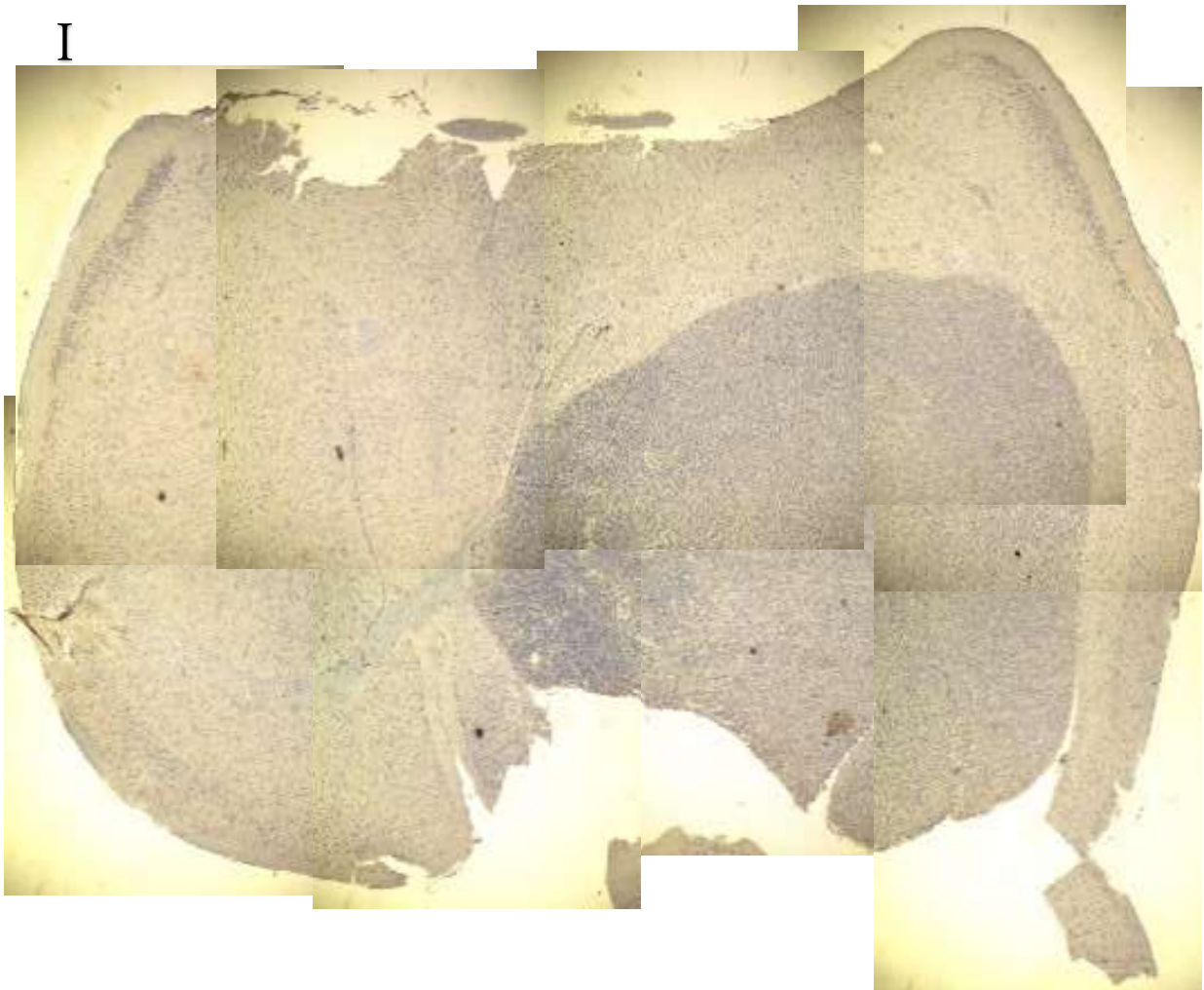
Figure. 3.5. Macroscopic images of SorLA and Aβ expression in mouse xenograft brain tissue: SorLA with haematoxylin (A, B, C); Aβ with hematoxylin (D, E, F); and IgG (G, H, I).

Plaques of both SorLA (A-C) and Aβ (D-F) are evident (*) throughout the tumour. Within the tumours are regions absent of immunoreactivity, where the needle penetrated to graft U87MG cells causing damage (white arrows). Additionally, a visible halo region of marked Aβ immunoreactivity was seen in the non-tumour tissue surrounding the tumour (arrowheads). Marked Aβ immunoreactivity was seen in non-tumour tissue surrounding the tumours. Scale bars 100μm, mag x10, n=3.
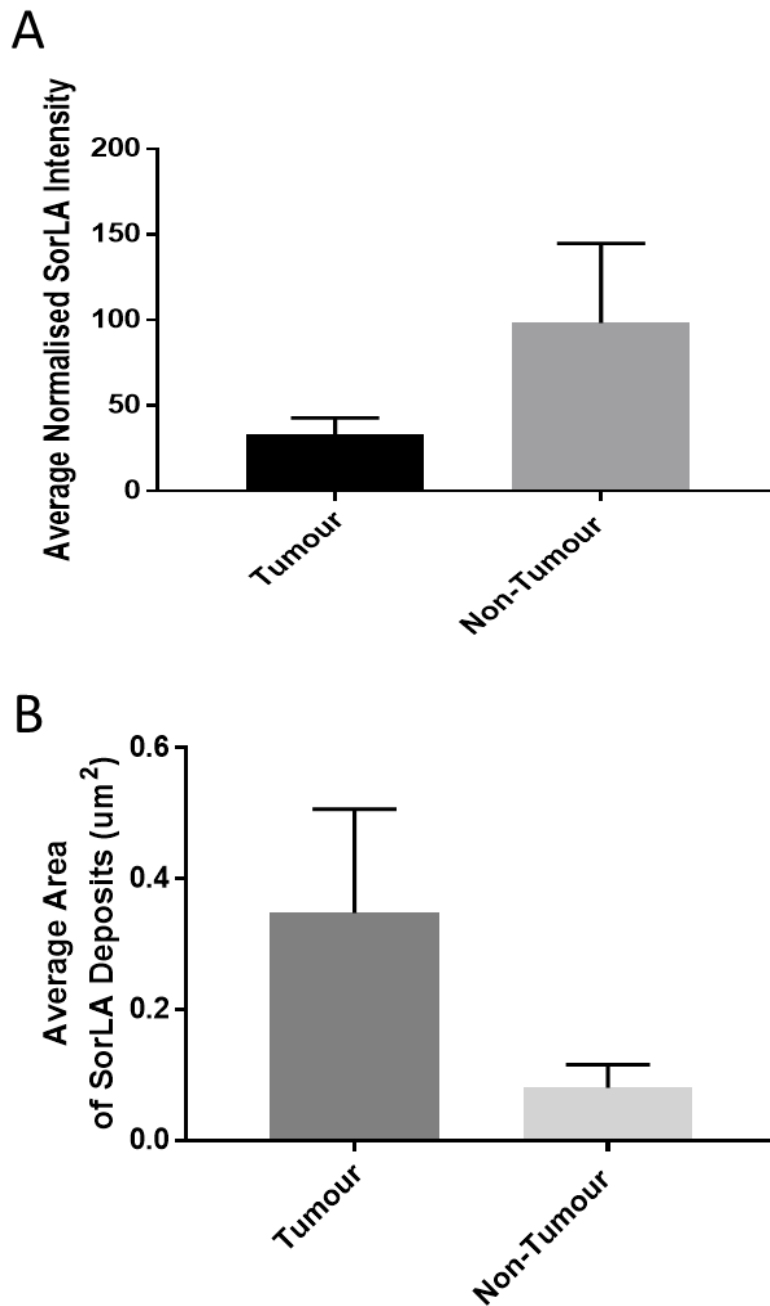
Figure 3.6. Compiled mean greyscale density (A) and mean area of SorLA deposits (B) between tumour and non-tumour tissue areas. SorLA immunoreactivity was significantly higher in tumour tissue ($p<0.001$ paired t-test, n=3). SorLA plaque size was also significantly higher within the tumour than in non-tumour tissue ($p<0.01$ paired t-test, n=3). Tabulated in Appendix 12.
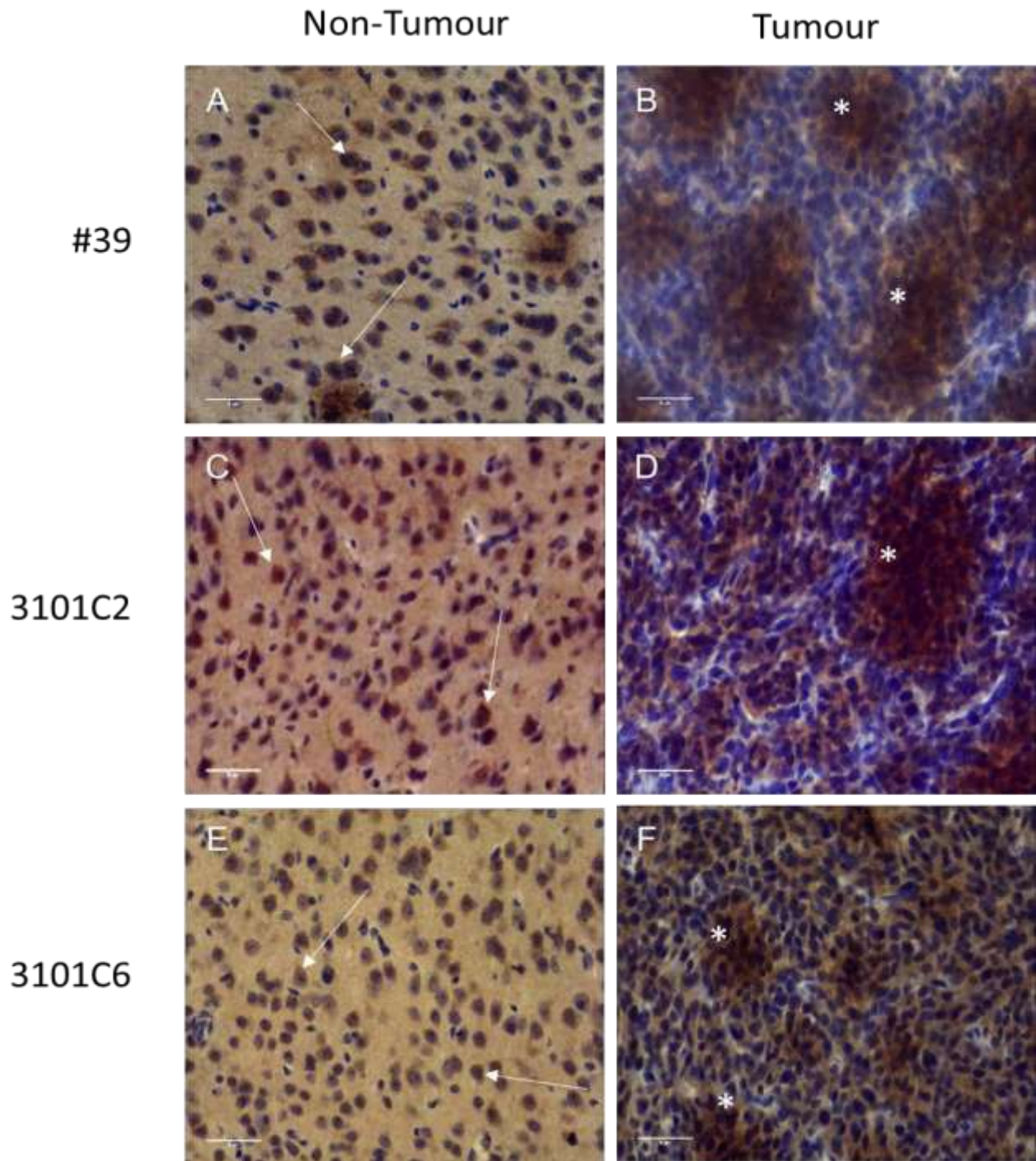
Figure 3.7. SorLA expression in tumour and non-tumour regions of mouse U87MG xenograft brain tissue. Non-tumour regions (A, C, E) showed predominantly intracellular SorLA expression (white arrows), contrasted by haematoxylin to indicate nuclei position. Some extracellular deposition is evident in A, though across the non-tumour region it was not as widespread or dense as the tumour region. Tumour tissue (B, D, F) showed extensive SorLA deposition in extracellular plaques (*). Replicate data can be found in Appendix 6. Scale bars 50 μm. Mag x40.

3.5. Immunohistochemical localization of amyloid beta in mouse tumour

3.5.1. Amyloid beta expression in mouse tumour brain

Aβ immunoreactivity was seen throughout the brains tested in tumour and non-tumour regions in all three mice (Figure 3.5). Like SorLA, highly stained localised regions of Aβ were seen within the tumour. Similar again to SorLA, plaques of Aβ were evident in tumour regions. Interestingly, plaques were also seen in non-tumour regions, although they were significantly larger in tumour tissue than non-tumour tissue (Figure 3.9 A, M = 0.189, SD = 0.115, SEM = 0.012); $t(89) = 15.63$, $p<0.001$).

There was, however, marked variation between animals with one mouse brain showing large highly immunoreactive Aβ plaques (Figure 3.5 D), also demonstrating the lightest SorLA staining within the tumour (Figure 3.5, A). Conversely, the other two tumours showed heavier SorLA staining and lighter Aβ immunoreactive plaques (Figure 3.5 B vs E and C vs F). One noteworthy observation therefore was the possible trend towards an inverse correlation between SorLA expression and Aβ expression, with high SorLA tumour expression seeming to be associated with lower Aβ expression.

Densitometric analysis between tumour and non-tumour tissue staining intensity showed a significant difference similar to SorLA (Figure 3.8 B, M = 32.71, SD = 22.75, SEM = 5.36); $t(17) = 6.1$, $p < 0.001$). There was however a marked difference in the pattern of immunostaining in the non-tumour tissue with Aβ evident in the tissue immediately surrounding the tumour. This Aβ staining formed a "halo" around the tumour with the most intense staining immediately adjacent to the tumour margin that decreased as the distance from the tumour increased (Figure 3.9). Line scans of Aβ immunoreactivity gave a visual representation of the decrease in staining intensity with increasing distance from the tumour margin.

Three times per brain, lines were randomly drawn perpendicular to the tumour margin and a greyscale value was calculated for every point along that line. Higher values represent a greater degree of 'whiteness' in the image, hence a lower level of DAB staining (Figure 3.9).

Line lengths were intended to be equal for all brains, however the 3101C2 mouse line length was necessarily shorter than the others due to the smaller size of this brain. The line scans demonstrated a strong positive correlation between image 'whiteness' and distance from tumour for all the mouse brains, representative of a proportionate decrease in Aβ staining with increasing distance from the tumour margin (#39, r = 0.9773, p<0.001; 3101C2, r = 0.9405, p<0.001; 3101C6, r = 0.9623, p<0.001).

At higher magnification the extracellular nature of the tumour beta-amyloid positive plaques was evident. Moreover, strong immunostaining was seen to form a 'thread-like' pattern between tumour cells (Figure 3.10, B, D & F, arrows) that was not seen in non-tumour tissue.
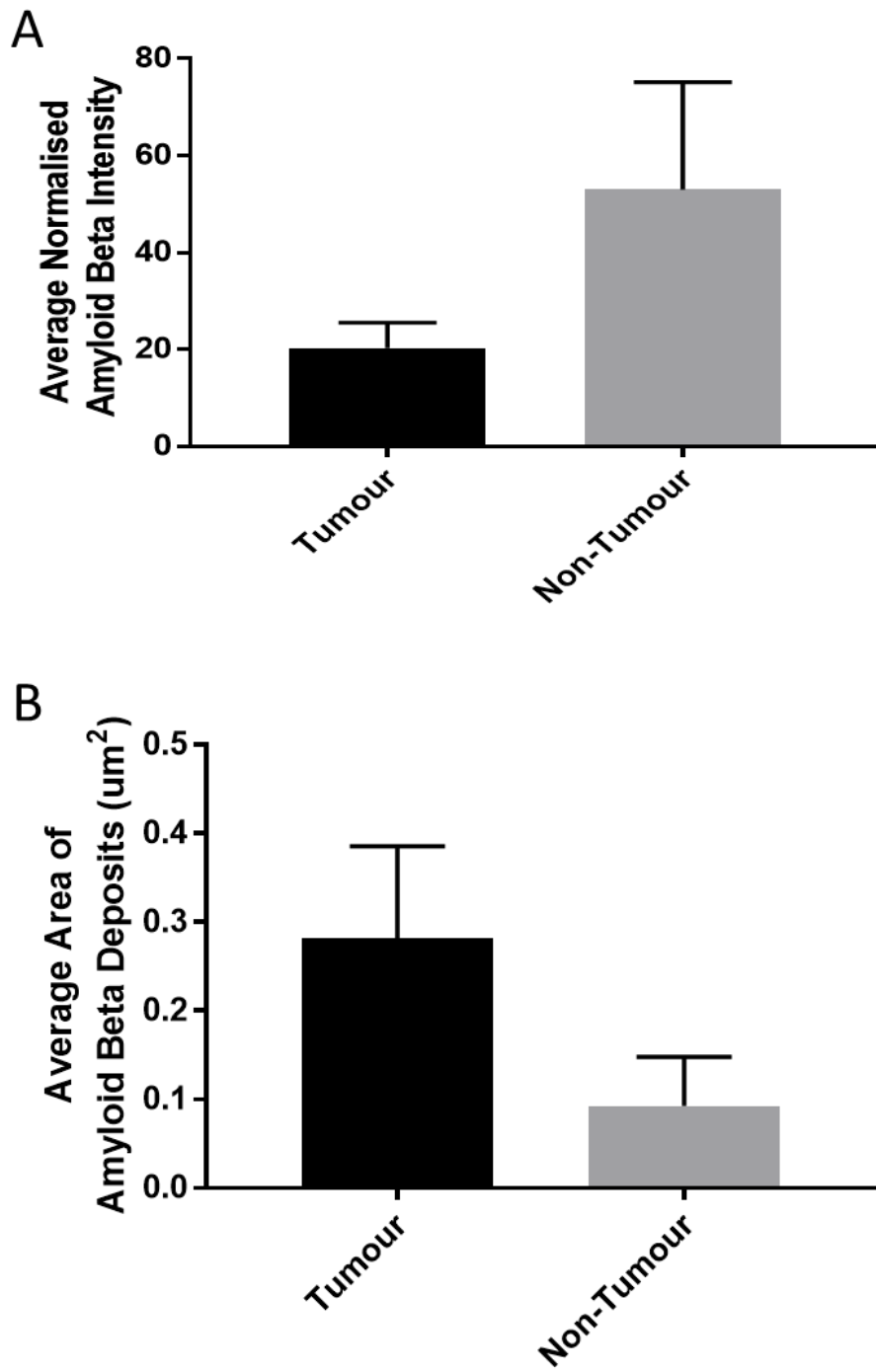
Figure 3.8. Intensity and significance of Aβ plaques inside vs outside the tumour (A), and the Aβ plaque area (B). The mean intensity between Aβ plaques within and without the tumour (B) was compared; as well as the area of Aβ plaques (μm^2). Tabulated in Appendix 13. FOV=3, n=3.
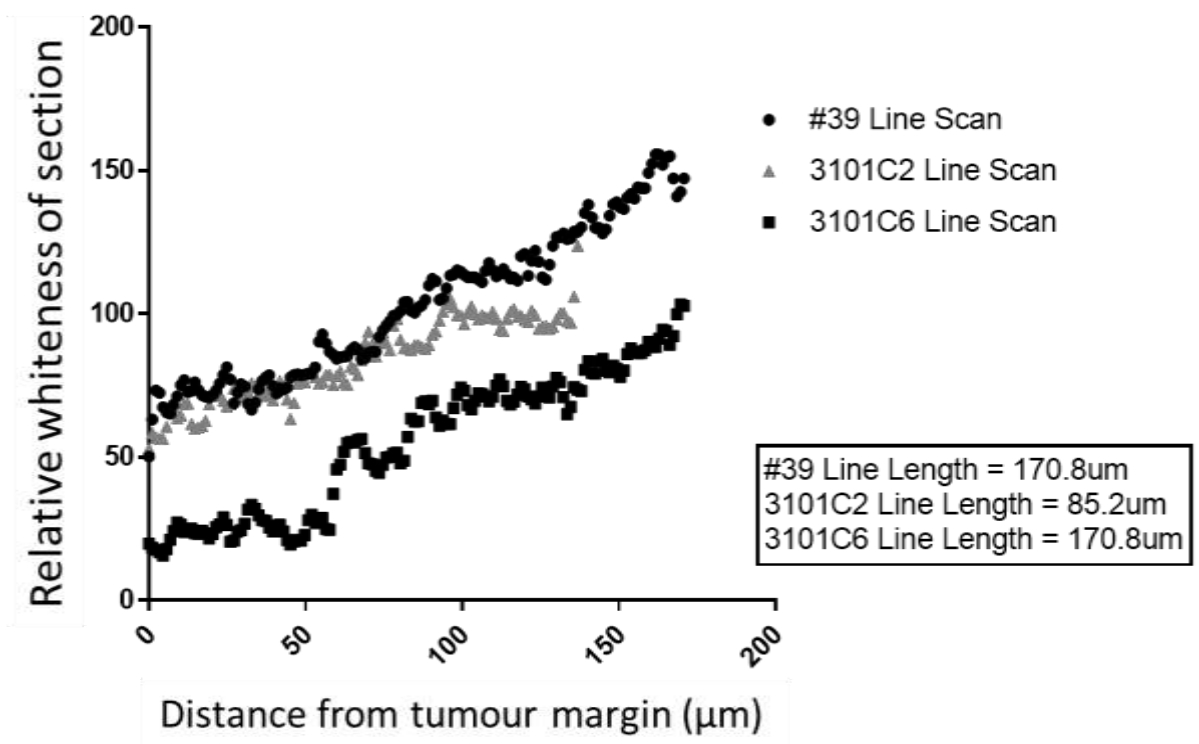
Figure 3.9. Greyscale intensity at increasing distance perpendicular from tumour margin.

A Pearson r test found a significant positive correlation in all the line scans, indicating a significantly reduced Aβ immunoreactivity with increasing distance from the tumour margin; #39 (r = 0.9773, p<0.001); 3101C2 (r = 0.9405, p<0.001); 3101C6 (r = 0.9623, p<0.001).

	Non-Tumour	Tumour
#39		
3101C2		
3101C6		
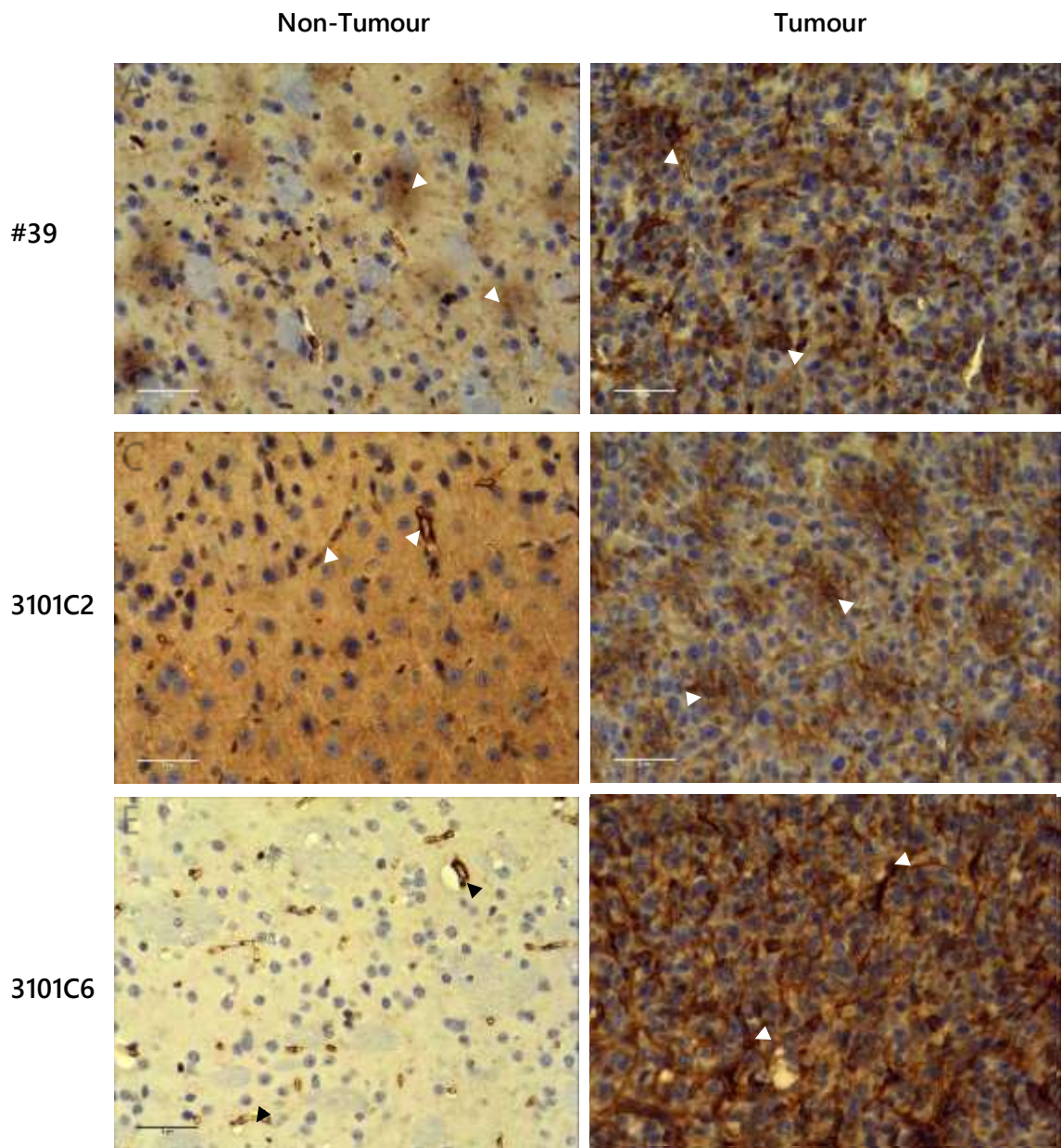
Figure 3.10. Aβ expression in tumour and non-tumour regions of mouse U87MG xenograft brain tissue. Non-tumour regions (A, C, and E) showed extracellular immunoreactivity of Aβ (arrowheads). Tumour regions (B, D, and F) demonstrated enhanced Aβ immunoreactivity and the presence of thread-like extracellular plaques between cells (white arrows). Replicate data can be found in Appendix 7. Scale bar, 50 μm. Mag x40.

CHAPTER 4

DISCUSSION

The thesis hypothesis was that, in glioma, intracellular expression of SorLA is upregulated and Aβ is decreased. This was tested through analysis of SorLA expression via IF on human glioma cell lines *in vitro* and by IHC for SorLA and Aβ in brain sections from murine glioblastoma models. Importantly, initial H&E staining confirmed the presence of sizeable tumours within the mouse model brain sections in the right lobe of the anterior region.

Overall, the hypothesis was not achieved, with IF data suggesting a normal distribution and non-significant difference of intracellular SorLA between NHAs and the glioma cell lines. Though this is compounded by the limitations of the techniques and the methods unable to be used such as more accurate protein quantification through WB for example. As well as the issue of the extracellular SorLA in the tumour regions making it impossible to accurately discern between SorLA within and outside of the cells on the IHC samples.

Furthermore, the amyloid beta expression in the brain samples showed a clear difference between the tumour and non-tumour tissue. Again, running counter to the hypothesis. However, the results achieved do show potential for future avenues of work.

4.1.   Relative SorLA expression *in vitro*

SorLA immunoreactivity was evident in both astrocyte cell types tested, in keeping with previous reports that it is expressed throughout the nervous system (Willnow and Andersen, 2013; Schmidt & Willnow, 2016). Moreover, SorLA was similarly visualised by IF in both human glioma cell lines tested – U87-MG and T98G – supporting previous studies which saw expression in glioma cell lines (Salgado *et al.,* 2012). The highest level of SorLA immunofluorescence intensity per cell was found in NHAs – primary human astrocytes derived from foetal tissue - in all three experimental repeats. Conversely, the lowest level per cell was seen in the human foetal astrocyte cell line SVGp12. These differences, although not significant, may be attributed to the relative size of these cell types skewing the results. SVGp12 cells are of a standard cell line size and shape, with cell bodies typically 20-30 µm across and exhibiting

only a small degree of short process growth (Major *et al.,* 1985). The highly heterogenous primary NHA cells were markedly larger, with cells often reaching over 100 μm in diameter and frequently sending out long processes. Hence, differences in the amount of SorLA present may simply be a function of relative cell volumes. Another method therefore for quantifying expression as a function of area rather than on a per cell basis may have helped smooth these inequalities out, however given the complex cell shapes involved (most notably for the NHA) development of such an analysis protocol within the timescale of the project was unfeasible. Alternatively, these discrepancies could have been due to the nature of the foetal astrocyte cell types tested. While the NHA cells used are certified as astrocytic and have been validated as such in our lab, the SVGp12 cell line has been speculated to comprise neural progenitor cells, which might explain their morphological dissimilarity to primary human astrocytes *in vitro* (Dowling-Warriner and Trosko, 2000). A further limitation of the NHA control used however, is that they are not as accurate to make a comparison from as samples taken from non-glioma affected mice/patients. This is due to the NHAs being grown in conditions different to those that would be found *in vivo*. Although, this would bring up the issue of the glioma cells tested also not being as representative as glioma cells of the same type being xenografted and grown in mouse subjects.

Ultimately there was no significant difference in SorLA expression found between either of the control astrocyte cell types and the two glioblastoma cell lines using this methodology. Notwithstanding the above, this is at odds with both the hypothesis of the thesis and findings of Lui *et al.,* (2016) who reported decreased SORL1 mRNA expression in clinical astrocytoma samples. Importantly however, these results did confirm the expression of SorLA in the U87-MG cells which were the basis for the murine xenograft model to be utilised for the remainder of the project.

While direct quantification of relative protein amounts using WB would have been preferable to IF to compare protein levels *in vitro*, despite significant time and effort reliable blots could

not be produced within the timescale of the project. Multiple antibodies from different suppliers were tested and yielded no bands, streaks or bands of inconsistent size. It was postulated that being a transmembrane protein, SorLA may have been incompletely solubilised by the RIPA buffer-based lysis method employed, hence a harsher urea-based method (Ngoka, 2008) was tested but this also failed to provide clean blots. Given that the experimental plan for this work was always meant to include IHC in murine xenograft glioblastoma models, and such whole-tumour work is arguably of greater significance to test the hypotheses of the project than glioma cell lines *in vitro*, a decision to move on to the next stage of the project was taken.

4.2.   Subcellular distribution of SorLA is unaltered in glioma

SorLA intracellular pattern immunoreactivity within both non-cancerous astrocyte cell types was punctate and consistent with the localisation of endomembranes and the plasma membrane, in keeping with the published role of SorLA as a transmembrane trafficking protein which moves between cellular compartments (Hermey, 2009; Schmidt & Willnow, 2016). Crucially, the two glioblastoma cell lines tested exhibited an indistinguishable subcellular distribution of SorLA by IF, suggesting that SorLA's membrane distribution is not overtly affected by the transformation of astrocytes to a glioma phenotype. Notwithstanding, while the methodology utilised can give a good overview of protein distribution (i.e. it can confirm that SorLA has not been uniquely targeted to a single cellular compartment, such as the lysosomes, for example), it was not possible to quantify the relative proportion of SorLA in each compartment. A modest shift in the relative amount of SorLA present in each of the intracellular compartments could conceivably have repercussions for the proper proteolytic processing of APP (Willnow and Andersen, 2013), altering the ratio of Aβ40:Aβ42 (Murphy and LeVine, 2010; Kamentani and Hasegawa, 2018), and/or affect the uptake and degradation of Aβ (Eggert et al., 2017). Hence, although these results do indicate that SorLA is still present and

localises to the correct cellular compartments in glioma *in vitro*, further investigation will be required to confirm whether or not there are any more subtle disturbances, which may have pathological implications.

4.3.   Tissue expression of SorLA in mouse brain

SorLA expression has a widespread distribution in both nervous and non-nervous tissue (Jiang *et al.,* 2016; Højland *et al.,* 2018) with a neuronal distribution localised to the somatodendritic domain (Klinger *et al.,* 2016). The present study also showed widespread SorLA with a relatively uniform expression across non-tumour tissue. Where strongly labelled SorLA was seen in non-tumour tissue it was likely intracellular, matching the distribution of SorLA in non-AD control brain samples in a study by Thonberg and colleagues (2017). It is interesting to note that SorLA positive plaques were also reported, albeit to a lesser degree than the tumours here, in post-mortem brain tissue from patients with Alzheimer's disease (Thonberg *et al.,* 2017).

SorLA exists as an intracellular transmembrane receptor, typically linked to the Golgi network and endosomes but can also shed an ectodomain through intramembrane proteolysis to yield soluble SorLA (sSorLA) releasing it from the cell as the cytoplasmic tail is shed (Terai *et al.,* 2016). It is unclear which form is being picked up here but is likely to be the sSorLA as the antibody targets a region of class A repeats between 1350-1550 amino acids, and not the cytoplasmic tail motif (UniProt, 2017). Unfortunately, no selective antibodies for the two forms are currently commercially available.

4.3.1.   SorLA presence and expression in glioma

A link between SorLA and cancer was speculated a number of years ago, with an initial report describing a role of SorLA in proliferation and differentiation of neuroblastoma (Hirayama *et al.,* 2000). The soluble form, that can be retrieved from plasma, was later linked to various

cancers, lymphoma in particular (Terai *et al.,* 2014; Fujimura *et al.,* 2014; Kawaguchi *et al.,* 2015; Sugita *et al.,* 2016) giving rise to the possibility that it may have potential as a novel biomarker. The SorLA staining in the plaques here appeared to be extracellular so when considered with the reported findings of sSorLA shedding in other cancers, it is likely that the staining here is also soluble SorLA. However, in the previous lymphoma reports, sSorLA was found alongside enhanced SorLA transcription (Fujimura *et al.,* 2014; Ohwada *et al.,* 2015), a consideration for future work. That SorLA can be upregulated at the transcriptional level may also tie in with reports suggesting sSorLA acts as a hypoxia-induced migration inducer (Nishii *et al.,* 2013). It might be expected that the xenografts induced here would develop hypoxic regions and a necrotic core, characteristic hallmarks of glioblastoma (Joseph *et al.,* 2015), to drive an increased SorLA expression. In contrast however, whilst there may be enhanced shedding, the macroscopic images of the murine models show no consistent discernible presence of necrosis, and a relatively uniform expression across the tumour. The increased SorLA expression may therefore indicates SorLA could have a more central role in cancer pathology, rather than appearing because of the tumour.

4.3.2. Tissue and tumour expression of amyloid beta

Significant Aβ staining was seen within the tumour and in the non-tumour tissue surrounding the tumour. The immunolabelling was abundant within the tumour in plaques, much like the extracellular SorLA. We can be confident that the plaques are indeed Aβ as such plaques have been found in other studies using the same anti-Aβ antibody (Vasilevko *et al.,* 2007; Walker *et al.,* 2009; Kai *et al.,* 2012; Edrey *et al.,* 2013; Sandoval-Hernández *et al.,* 2015). These plaques also appear to be of a similar size and morphology to those seen in murine models of AD (Oddo *et al.,* 2003). The plaques did not appear to co-localise with the SorLA plaques in near-adjacent tissue sections which is maybe not surprising as SorLA has been shown to have

an inverse correlation with beta amyloid expression in Alzheimer's brains. Future studies using co-labelling via immunofluorescence would be able to confirm the absence of any overlap.

4.3.3. Relationship between SorLA and amyloid beta

SorLA has a well characterised role regulating APP trafficking/processing (Hermey, 2009) where it carries out the retrograde transport and sorting of APP from the endosome, and back to the Golgi (Spoelgen *et al.,* 2006). This reduces the amyloidogenic processing of APP, despite only accounting for 10% of APP processing, because it is suggested to have an additional role in tagging monomeric Aβ for lysosomal degradation (Eggert *et al.,* 2017). This goes together with the results by Andersen et al. 2005, who found that SorLA knockout mice had significantly higher level of Aβ compared to wild-types. Consequently, data here may initially seem counterintuitive with tumour expressing levels of both SorLA AND amyloid beta. However, despite only being an anecdotal observation, it is worth noting that the mouse with lowest SorLA immunoreactivity had greatest amyloid beta immunoreactivity and two mice showed the opposite. It would be useful to explore the timecourse and establish the expression levels as the tumour develops to help shed light on the dynamic between SorLA and amyloid beta.

As the SorLA immunoreactivity seen is likely to be from the soluble form it seems reasonable to consider that intracellular levels of SorLA would be decreased. This would reduce APP being directed to the endosome and would thus be amyloidogenic. However, this is difficult to judge here as the strong SorLA labelling masks a lot of the glioma cells making it difficult to discern if there is less intracellular SorLA within the tumour.

4.3.4. Influence of amyloid beta on glioma

The effect increased expression of Aβ may have on glioma is currently unknown. Some previous studies have investigated APP in non-brain-associated cancers (thyroid, colon, pancreas, prostate) and reveal that APP is upregulated and involved in promoting oncogenic

effects including cell growth, proliferation and migration (Krause *et al.,* 2008; Takayama *et al.,* 2009; Venkataramani *et al.,* 2010; Lim *et al.,* 2014) with increased levels of APP associated with poor prognosis (Takayama *et al.,* 2009). Very few studies have looked at APP and glioma, although it has been reported that there is a significant increase in APP seen in the U87MG glioma cell line (Guo *et al.,* 2017). This supports our data here as an increase in APP within tumour could lead to a rise in Aβ production if there was a lack of intracellular SorLA expression to aid in normal APP processing to the endosome.

Only a small number of studies have considered an interaction between amyloid beta and tumours, and glioma in particular. It has previously been demonstrated that Aβ can inhibit glioma cell growth *in vitro* (Zhao *et al.,* 2009, Youn *et al.,* 2015) and that glioma cells grow more slowly when injected into the brains of AD mice models who overproduce Aβ (Paris et al. 2010). The anti-cancer effect of Aβ isn't limited to brain tumours however as a fragment of Aβ also decreased proliferation and tumour vascularisation in a mouse model of breast cancer (Paris *et al.,* 2010). Amyloid beta may therefore have anti-tumour properties and raises the possibility that Aβ is produced as a response to the tumour to try and inhibit tumour growth. This hypothesis is supported by a small study on human post mortem tissue that showed a lower proportion of AD plaques in *post-mortem* tissue from glioblastoma patients than from non-glioblastoma patients (Nelson 2002). An anti-cancer effect of Aβ has been speculated to occur through inhibition of formation of new blood vessels (Patel *et al.,* 2010, Paris et al. 2015), although this remains unresolved as a pro-angiogenic effect of Aβ has also been reported (Cameron *et al.,* 2012). The reported increase in APP seen in glioblastoma tissue (Culicchia *et al.,* 2008) would also support an Aβ-mediated anti-tumour response from the tissue but would contrast starkly with the oncogenic properties of APP reported above in other tumour types. Whether this is a feature specific to glioma remains to be determined.

It is interesting to note that the putative antitumour effects of amyloid beta may correspond with epidemiological data suggesting a co-morbidity and an inverse correlation between AD

and cancer (Musicco *et al.,* 2013, Catala-Lopez *et al.,* 2014, Shi *et al.,* 2014). This is countered however by other studies which proclaim that AD and glioma are instead positively correlated (Lehrer S. 2018). A host of genes were identified via transcriptomic meta-analysis, finding a similar pattern of changes on them in AD and glioblastoma, with the study further analyzing these affected genes, seeing that they were deregulated and linking them to mitochondrial dysfunction (Sánchez-Valle *et al.,* 2017). This dysfunction was thought to lead to an increase in reactive oxygen species production, a known change in AD brains mainly (Silva *et al.,* 2011). Though, further affecting mitochondria function, they did find that 10 mutated genes are shared between the diseases, finding them to involved in downregulating oxidative phosphorylation and upregulating interferon alpha beta induction. Together this supported a hypothesis of a localized chronic inflammatory state occurring, a feature other studies have demonstrated as promoting tumour development (Lu *et al.,* 2006; Galvão and Zong, 2013; Mcdonald *et al.,* 2017). Also, the lack of oxidative phosphorylation in cells within the brain, means a lower rate of mitochondrial energy production, thus leading to synaptic transmission dysfunction (Pathak *et al.,* 2015).

The contribution Aβ makes to the pathogenesis of AD is complicated by the different peptides generated from APP as various enzymes cleave it in different places (Luo *et al.,* 2016, Andrew *et al.,* 2016). APP is severed by a first enzyme (β-secretase) and one of the fragments is then trimmed by a second enzyme (γ-secretase) complex to produce a 40 amino acid long Aβ40 peptide (Andrew *et al.,* 2016). This peptide is relatively benign and may be involved in neuronal survival and modulating synaptic activity (Mordhwaj *et al.,* 2011). However incomplete trimming of the fragment yields a longer Aβ42 peptide that is more prone to aggregating and makes a major contribution to the hallmark amyloid plaques seen in brains of AD patients (Takami *et al.,* 2009). It is unfortunate that the previous studies linking cancer/glioma and Aβ did not specify which isoform of amyloid beta was studied. Consequently, we can only speculate which isoform was picked up here as the antibody

employed also could not differentiate between Aβ40 and Aβ42. As the immunoreactivity was seen in plaques and as SorLA is likely to be soluble and extracellular, it therefore seems likely that the immunoreactivity seen here would be the fibrillogenic Aβ42 form, rather than Aβ40.

4.3.5. Amyloid beta expression peripheral to the tumour

Data here show marked amyloid beta deposition in the tissue surrounding the tumour. To our knowledge, this is the first time such an observation has been seen. The amyloid beta halo region surrounding the tumour in the mouse brain sections are distinct in that Aβ intensity declines the greater the distance from the tumour edge. The source of this Aβ is open to speculation and could either be from the non-tumour tissue or from the tumour itself. As Aβ plaques have been suggested to have a role as a protective 'reservoir' of soluble Aβ aggregates (Esparza *et al.,* 2018) it's possible that the Aβ halo region starts from the non- tumour and increases closer to the tumour as a defensive response to prevent exfiltration and keep sequestered the soluble Aβ plaques. Conversely it may be that the Aβ may be from the tumour and there is infiltration into non-tumour tissue of soluble Aβ due to it overwhelming the plaques within the tumour acting as a buffer. Amyloid beta halos have been reported previously, on a much a smaller scale, as soluble oligomeric Aβ halos were seen to surround synapses and contribute to synaptic loss in AD (Koffie *et al.,* 2009; 2012).

CHAPTER 5

CONCLUSION

5.0.   Conclusion

This investigation demonstrated the presence of SorLA in glioma cell lines and in U87MG xenograft, and that SorLA, likely sSorLA, formed apparent extracellular plaques within the tumour. In addition, the study found that amyloid beta was also present in tumour tissue in the form of extracellular plaques and in non-tumour tissue immediately peripheral to the tumour. However, these unexpected results run counter to the hypothesis, though the aims of the thesis were achieved.

CHAPTER 6

FUTURE WORK AND DIRECTION

6.0.   Future work and direction

The work carried out here is an interesting preliminary investigation into SorLA and Aβ's role in glioma and supports further work be done in the area. The obvious next question is to determine which types of Aβ are present within the tumour as the primary anti-Aβ antibody used here reacts to the 1-16 amino acid residue, meaning it is impossible to distinguish the Aβ seen between the Aβ40 and/or Aβ42 types. This could be accomplished by using the more specific Aβ antibodies that are commercially available.

Future work should establish if the SorLA detected in the extracellular space is sSorLA. This would go towards validating the idea that there may be enhanced proteolytic shedding of SorLA within the glioma cells. One way to do this would be through sSorLA ELISA kits upon various glioma short term primary culture and glioma cell line media, and their corresponding lysates, alongside NHAs to provide a comparison, as it would quantify the amount both intra- and extracellularly. To expand upon this in context of the work already done, would be to do the same for Aβ in glioma cell lines and STC lysate and medium too.

In the context of what was discussed in the previous chapter, APP expression could be investigated to confirm the reported upregulation within glioma cells. This should utilise western blotting detection of NHAs, multiple glioma cell lines and STC lysates to enable a greater comparison and lend validity to any conclusions drawn. ELISA upon the lysates to quantify the levels APP and SorLA would provide additional evidence also.

To further enhance the results that might be obtained from the ELISA in determining intracellular and extracellular levels of sSorLA, FACS would be allow for an understanding of whether SorLA is expressed within the glioma cells in comparison to NHAs for example.

To test the idea that sSorLA is a hypoxia-induced migration inducer, glioma cell lines/STCs could be grown in a hypoxic chamber and the culture medium measured for sSorLA levels at varying intervals through a combination of FACS and ELISA.

This project did not look at the tumour development and its relation to SorLA and Aβ expression. As such, future work in this regard may incorporate a longitudinal study to determine expression of SorLA and amyloid beta as the tumour develops. In particular this may help understand whether the amyloid beta is present in non-tumour tissue as a consequence of the tumour or emanate from the tumour itself.

An inherent limitation of using U87MG cell lines is that it is not human glioma tissue. Utilising human patient biopsy tissue would add much validity to the study here if the findings were mirrored in human tissue. Acquiring tissue of varying age groups, genders, and glioma grades would yield important data as expression could be correlated to the various patient groups available. SorLA and amyloid beta can both exist as soluble forms with the potential to be released. This is particularly significant given the suggestion that Aβ can be detected in plasma (Roher et al. 2009) and therefore could have biomarker potential for AD which may indicate potential for it to also be a biomarker for glioma as well.

CHAPTER 7

REFERENCES

Ables J. L., Breunig J. J., Eisch A. J., Rakic P. 2011. Not(ch) just development: Notch signalling in the adult brain. *Nature Reviews. Neuroscience.* 12(5): 269-283.

Andersen O. M., Reiche J., Schmidt V., Gotthardt M., Spoelgen R., Behlke J., von Arnim C. A., Breiderhoff T., Jansen P., Wu X., Bales K. R., Cappai R., Masters C. L., Gliemann J., Mufson E. J., Hyman B. T., Paul S. M., Nykjaer A., Willnow T. E. 2005. Neuronal Sorting Protein-Related Receptor SorLA/LR11 Regulates Processing of the Amyloid Precursor Protein. *Proceedings of the National Academy of Sciences of the United States of America.* 102: 13461-13466.

Anjum K., Shagufta B. I., Abbas S. Q., Patel S., Khan I., Shah S. A. A., Akhter S., ul Hassan S. S. 2017. Current status and future therapeutic perspectives of glioblastoma multiforme (GB) therapy: A Review. *Biomedicine & Pharmacotherapy.* 92: 681-689.

Banerjee G., Carare R., Cordonnier C., Greenberg S. M., Schneider J. A., Smith E. E., van Buchem M., van der Grond J., Verbeek M. M., Werring D. J. 2017. The increasing impact of cerebral amyloid angiopathy: essential new insights for clinical practice. *Journal of Neurology, Neurosurgery, and Psychiatry.* 88(11): 982-994.

Benveniste E. N., Sparacio S. M., Norris J. G., Grenett H. E., Fuller G. M. 1990. Induction and regulation of interleukin-6 gene expression in rat astrocytes. *Journal of Neuroimmunology*. 30(2-3): 201-212.

Böhm C., Seibel N.M., Henkel B., Steiner H., Haass C., Hampe W. 2006. SorLA signaling by regulated intramembrane proteolysis. *Journal of Biological Chemistry*. 281(21):14547-53.

Brothers H. M., Gosztyla M. L., Robinson S. R. 2018. The Physiological Roles of Amyloid-β Peptide Hint at New Ways to Treat Alzheimer's Disease. *Frontiers in Aging Neuroscience.* 10: 118.

Catalá-López F., Suárez-Pinilla M., Suárez-Pinilla P., Valderas J. M., Gómez-Beneyto M., Martinez S., Balanzá-Martínez V., Climent J., Valencia A., McGrath J., Crespo-Facorro B., Sanchez-Moreno J., Vieta E., Tabarés-Seisdedos R. 2014. Inverse and direct cancer comorbidity in people with central nervous system disorders: a meta-analysis of cancer incidence in 577,013 participants of 50 observational studies. Psychotherapy and Psychosomatics. 83(2):89-105.

Chen W., Xia T., Wang D., Huang B., Zhao P., Wang J., Qu X., Li X. 2016. Human Astrocytes Secrete IL-6 to Promote Glioma Migration and Invasion Through Upregulation of Cytomembrane MMP14. *Oncotarget.* 7(38): 62425-62438.

Codeluppi S., Fernandez-Zafra T., Sandor K., Kjell J., Liu Q., Abrams M., Olson L., Gray N. S., Svensson C. I., Uhlén P. 2014. Interleukin-6 Secretion by Astrocytes Is Dynamically Regulated by PI3K-mTOR-Calcium Signaling. *PLoS One*. 9(3).

Dawkins E., Small D. H. 2014. Insights into the physiological function of the β-amyloid precursor protein: beyond Alzheimer's disease. *Journal of Neurochemistry*. 129(5): 756-769.

Dowling-Warriner C. V., Trosko J. E. 2000. Induction of gap junctional intercellular communication, connexin43 expression, and subsequent differentiation in human fetal neuronal cells by stimulation of the cyclic AMP pathway. Neuroscience 95:859 –868.

Du X., Wang X., Geng M. 2018. Alzheimer's disease hypothesis and related therapies. *Translational Neurodegeneration.* 7: 2.

Eggert S., Gonzalez A. C., Thomas C., Schilling S., Schwarz S. M., Tischer C., Adam V., Strecker P., Schmidt V., Willnow T. E., Hermey G., Pietrzik C. U., Koo E. H., Kins S. 2017. Dimerization leads to changes in APP (amyloid precursor protein) trafficking mediated by LRP1 and SorLA. *Cellular and Molecular Life Sciences.* 01-22.

Ensembl. (2017). Gene: SORL1 ENSG00000137642. Available: http://www.ensembl.org/Homo_sapiens/Gene/Summary?db=core;g=ENSG00000137642;r=11:121 452203-121633693. Last accessed 08th Dec 2017.

Esparza T. J., Gangolli M., Cairns N. J., Brody D. L. 2018. Soluble amyloid-beta buffering by plaques in Alzheimer disease dementia versus high-pathology controls. *PLoS One*.3(7):e0200251.

Fujimura K., Ebinuma H., Fukamachi I., Ohwada C., Kawaguchi T., Shimizu N., *et al*. 2014. Circulating LR11 is a novel soluble-receptor marker for early-stage clinical conditions in patients with non-Hodgkin's lymphoma. *Clinica Chimica Acta*. 430:48-54.

Galvão R. P., Zong H. 2013. Inflammation and Gliomagenesis: Bi-Directional Communication at Early and Late Stages of Tumor Progression. *Current Pathobiology Reports*. 1(1): 19-28.

Gokden M. 2017. If it is not a Glioblastoma, Then What is it? A Differential Diagnostic Review. *Advances in Anatomic Pathology*. 24(6): 379-391.

Guan J., Mishra S., Falk R. H., Liao R. 2011. Current perspectives on cardiac amyloisosis. *American Journal of Physiology Heart and Circulatory Physiology*. 302(3): H544-H552.

Guo Y., Zhang P., Zhang H., Zhang P., Xu R. 2017. RNAi for contactin 2 inhibits proliferation of U87-glioma stem cells by downregulating AICD, EGFR, and HES1. OncoTargets and Therapy. 10: 791-801.

Gustafsen C., Glerup S., Pallesen L. T., Olsen D., Andersen O. M., Nykjær A., Madsen P., Petersen C. M. 2013. Sortilin and SorLA Display Distinct Roles in Processing and Trafficking of Amyloid Precursor Protein. *Journal of Neuroscience*. 33(1): 64-71.

Hardy J. A., Higgins G. A. 1992. Alzheimer's disease: the amyloid cascade hypothesis. *Science*. 256(5054):184-5.

Herskowitz J. H., Offe K., Deshpande A., Kahn R. A., Levey A. I., Lah J. J. 2012. GGA1-Mediated Endocytic Traffic of LR11/SorLA alters APP Intracellular Distribution and Amyloid-Beta Production. *Molecular Biology of the Cell*. 23: 2645-2657.

Hermey G., Sjøgaard S.S., Petersen C.M., Nykjaer A., Gliemann J. 2006. Tumour necrosis factor alpha-converting enzyme mediates ectodomain shedding of Vps10p-domain receptor family members. *Biochemical Journal*. 395(2):285-93.

Hermey G. 2009. The Vps10p-domain receptor family. *Cellular and Molecular Life Sciences*. 66(16):2677-89.

Hirayama S, Bujo H., Yamazaki H., Kanaki T., Takahashi K., Kobayashi J., *et al*. 2000 Differential expression of LR11 during proliferation and differentiation of cultured neuroblastoma cells. *Biochem Biophys Res Commun*. 275: 365-373.

Jiang L., Konishi H., Nurwidya F., Satoh., Takahashi F., Ebinuma H., Fujimura K., Takasu K. Jiang M. Z., Shimokawa H. 2016. Deletion of LR11 attenuates hypoxia-induced pulmonary arterial smooth muscle cell proliferation with medial thickening in mice. *Arterio. Throm. Vasc. Biol*. 36: 1972-1979

Joseph J. V., Conroy S., Pavlov K., Sontakke P., Tomar T., Eggens-Meijer E., Balasubramaniyan V., Wagemakers M., den Dunnen W. F. A., Kruyt F. A. E. 2015. Hypoxia enhances migration and invasion in glioblastoma by promoting a mesenchymal shift mediated by the HIF1α–ZEB1 axis. *Cancer Letters*. 359(1): 107-116.

Kagan B. L., Jang H., Capone R., Teran Arce F., Ramachandran S., Lal R., Nussinov R. 2012. Antimicrobial properties of amyloid peptides. *Molecular Pharmaceutics*. 9(4): 708-717.

Kai H., Shin R-W., Ogino K., Hatsuta H., Murayama S., Kitamoto T. 2012. Enhanced Antigen Retrieval of Amyloid β Immunohistochemistry, Re-evaluation of Amyloid β Pathology in Alzheimer Disease and Its Mouse Model. *Journal of Histochemistry & Cytochemistry.* 60(10): 761-769.

Kametani F. and Hasegawa M. 2018. Reconsideration of Amyloid Hypothesis and Tau Hypothesis in Alzheimer's Disease. *Frontiers in Neuroscience.* 12: 25.

Kancha R. K., Stearns M. E., Hussain M. M. 1994. Decreased expression of the low density lipoprotein receptor-related protein/alpha 2-macroglobulin receptor in invasive cell clones derived from human prostate and breast tumor cells. *Oncology Research.* 6: 365-372.

Kawaguchi T., Ohwada C., Takeuchi M., Shimizu N., Sakaida E., Takeda Y., *et al*. 2013. LR11: a novel biomarker identified in follicular lymphoma. *British Journal of Haematology*. 163: 277-280.

Kazda T., Dziackt A., Burkon P., Pospisil P., Slavik M., Rehak Z., Jancalek R., Slampa P., Slaby O., Lakomy R. 2018. Radiotherapy of Glioblastoma 15 Years after the Landmark Stupp's Trial: More Controversies than Standards?. *Radiology and Oncology*. 52(2); 121-128.

Klinger S. C., Hojland A., Jain S., Kjolby M,. Madsen P., Svendsen A. D., Olivecrona G., Bonifacino J. S., Nielsen M. S. 2016. Polarized trafficking of the sorting receptor SorLA in neurones and MDCK cells *FEBS Journal*. 283: 2476-2493

Kozlowska A. K., Tseng H. C., Kaur K., Topchyan P., Inagaki A., Bui V. T., Kasahara N., Cacalano N., Jewett A. 2016. Resistance to cytotoxicity and sustained release of interleukin-6 and interleukin-8 in the presence of decreased interferon-γ after differentiation of glioblastoma by human natural killer cells. *Cancer Immunology, Immunotherapy.* 65(9): 1085-1097.

Larsen J. V., Kristensen A. M., Pallesen L. T., Bauer J., Vægter C. B., Nielsen M. S., Madsen P., Petersen C. M. 2016. Cytokine-Like Factor 1, an Essential Facilitator of Cardiotrophin-Like Cytokine: Ciliary Neurotrophic Factor Receptor α Signaling and sorLA-Mediated Turnover. *Molecular and Cellular Biology.* 36(8): 1272-1286.

Larsen J. V., Petersen C. M. 2017. SorLA in Interleukin-6 Signaling and Turnover*. Molecular and Cellular Biology*. 37(11): e00641-e00716.

Lehrer S. 2018. Glioma and Alzheimer's Disease. *Journal of Alzheimer's Disease Reports.* 2(1): 213-218

Lim S., Yoo B. K., Kim H-S., Gilmore H. L., Lee Y., Lee H-P., Kim S-J., Letterio J., Lee H-G. 2014. Amyloid-β precursor protein promotes cell proliferation and motility of advanced breast cancer. *BioMed Central Cancer*. 14: 928.

Liu Q., Li G., Li R., Shen J., He Q., Deng L., Zhang L., Zhang C., Zhang J. 2010. IL-6 Promotion of Glioblastoma Cell Invasion and Angiogenesis in U251 and T98G Cell Lines. *Journal of Neuro-Oncology.* 100(2): 165-176.

Liu Y., Beyer A., Aebersold R. 2016. On the Dependency of Cellular Protein Levels on mRNA Abundance. *Cell*. 165(3): 535-550.

Lopes M. B. S., Bogaev C. A., Gonias S. L., VandenBerg S. R 1994. Expression of α2-macroglobulin receptor/low density lipoprotein receptor-related protein is increased in reactive and neoplastic glial cells. *FEBS Letters.* 338: 301-305.

Louis D. N., Perry A., Reifenberger G, Deimling A. V., Figarella-Branger D., Cavenee W. K., Ohgaki H., Wiestler O. D., Kleihues P., Ellison D. W. 2016. The 2016 World Healthy Organization Classification of Tumors of the Central Nervous System: A Summary. *Acta Neuropathologica.* 131(6): 803-820.

Lu H., Ouyang W., Huang C. 2006. Inflammation, a key event in cancer development. *Molecular Cancer Research.* 4: 221-233.

Lukiw W. J., Cui J. G., Yuan L. Y., Bhattacharjee P. S., Corkern M., Clement C., Kammerman E. M., Ball M. J., Zhao Y., Sullivan P. M., Hill J. M. 2010. Acyclovir or Aβ42 peptides attenuate HSV-1-induced miRNA-146a levels in human primary brain cells. *Neuroreport.* 21(14): 922-927.

MacDonald T. J., Pollack I. F., Okada H., Bhattacharya S., Lyons-Weiler J. 2007. Progression-Associated Genes in Astrocytoma Identified by Novel Microarray Gene Expression Data Reanalysis. Methods in Molecular Biology. 377:203-222.

Major E. O., Miller A. E., Mourrain P., Traub R. G., de Widt E., Sever J. 1985. Establishment of a line of human fetal glial cells that supports JC virus multiplication. Proc. Natl. Acad. Sci. U. S. A. 82:1257–126

McCarthy B. J. 2011. Descriptive Epidemiology of Glioma. In: Mehta M. P., Chang S. M., Guha A., Newton H. B., Vogelbaum M. A. Principles and Practices of Neuro-Oncology: A Multidisciplinary Approach. United States of America: Demos Medical Publishing. 4-13.

McCarthy C, O'Gaora P, James WG, de Gaetano M, McClelland S, Fitzgerald DJ, Belton O. 2010. SorLA modulates atheroprotective properties of CLA by regulating monocyte migration. *Atherosclerosis.* 213(2): 400-407.

McDonald J. T., Gao X., Steber C., Breed J. L., Pollock C., Ma L., Hlatky L. 2017. Host mediated inflammatory influence on glioblastoma multiforme recurrence following high-dose ionizing radiation. *PLoS One.* 12(5): e0178155.

Mikkelsen V.E., Stensjøen A.L., Berntsen E.M., Nordrum I.S., Salvesen Ø., Solheim O., Torp S.H. 2017. Histopathological Features in Relation to Pretreatment Growth in Glioblastoma Patients. *World Neurosurgery.* 109:e50-e58.

Morwald S., Yamazaki H., Bujo H., Kusunoki J., Kanaki T., Seimiya K., Morisaki N., Nimpf J., Schneider W. J., Saito Y. 1997. A Novel Mosaic Protein containing LDL receptor elements is Highly Conserved in Humans and Chickens. *Arteriosclerosis, Thrombosis, Vascular Biology.* 17: 996-1002.

Murphy M. P. and LeVine III H. 2010. Alzheimer's Disease and the β-Amyloid Peptide. *Journal of Alzheimer's Disease.* 19(1): 311.

Musicco M., Adorni F., Di Santo S., Prinelli F., Pettenati C., Caltagirone C., Palmer K., Russo A. 2013. Inverse occurrence of cancer and Alzheimer disease: a population-based incidence study. *Neurology.* 81(4):322-8.

Nakata Z., Nagae M., Yasui N., Bujo H., Nogi T., Takagi J. 2011. Crystallization and preliminary crystallographic analysis of human LR11 Vps10p domain. *Acta Crystallographica, Section F, Structural Biology and Crystallization Communications.* 67(Pt 1): 129-132.

National Health Service. 2018. Alzheimer's Disease.
Available: https://www.nhs.uk/conditions/alzheimers-disease/. Last accessed 3rd Sep 2018.

National Institute of Neurological Disorders and Stroke. 2018. Alzheimer's Disease Information Page.
Available: https://www.ninds.nih.gov/Disorders/All-Disorders/Alzheimers-Disease-Information-Page. Last accessed 3rd Sep 2018.

Nishii, K., Nakaseko C., Jiang, M. Z., Shimizu N., Takeuchi M., Schneider W. J., Wolfgang J., Bujo H. J. 2012. The Soluble Form of LR11 Protein Is a Regulator of Hypoxia-induced, Urokinase-type

Plasminogen Activator Receptor (uPAR)-mediated Adhesion of Immature Hematological Cells. *Biol. Chem.* 288: 11877-11886.

Ngoka L. C. 2008. Sample prep for proteomics of breast cancer: proteomics and gene ontology reveal dramatic differences in protein solubilization preferences of radioimmunoprecipitation assay and urea lysis buffers. *Proteome Science*. 6:30-54.

O'Brien C. A., Lin S. C., Bellido T., Manolagas S. C. 2000. Expression levels of gp130 in bone marrow stromal cells determine the magnitude of osteoclastogenic signals generated by IL-6-type cytokines. *Journal of Cellular Biochemistry.* 79(4): 532-541.

Oddo S., Caccamo A., Shepherd J. D., Murphy M. P., Golde T. E., Kayed R., Metherate R., Mattson M. P., Akbari Y., LaFerla F. M. 2003. Triple-transgenic model of Alzheimer's disease with plaques and tangles: intracellular Abeta and synaptic dysfunction. Neuron. 39(3):409-21.

Ogita M., Miyauchi K., Dohi T., Tsuboi S., Miyazaki T., Yokoyama T., Yokoyama K., Shimada K., Kurata T., Jiang M., Bujo H., Daida H. 2013. Increased circulating soluble LR11 in patients with acute coronary syndrome. *Clinica Chimica Acta*.415:191-4.

Ostrom Q. T., Bauchet L., Davis F. G., Deltour I., Fisher J. L., Langer C. E., Pekmezci M., Schwartzbaum J. A., Turner M. C., Walsh K. M., Wrensch M. R., Barnholtz-Sloan J. S. 2014. The Epidemiology of Glioma in Adults: A "State of the Science" Review. *Neuro-Oncology.* 16(7): 896-913.

Pantoni L. 2010. Cerebral small vessel disease: from pathogenesis and clinical characteristics to therapeutic challenges. *The Lancet. Neurology.* 9(7): 689-701.

Paris D., Townsend K., Quadros A., Humphrey J., Sun J., Brem S., Wotoczek-Obadia M., DelleDonne A., Patel N., Obregon D. F., Crescentini R., Abdullah L., Coppola D., Rojiani A. M., Crawford F., Sebti S. M., Mullan M. 2004. Inhibition of angiogenesis by Abeta peptides. *Angiogenesis*. 7(1): 75-85.

Paris D., Ganey N., Banasiak M., Laporte V., Patel N., Mullan M., Murphy S. F., Yee G. T., Bachmeier C., Ganey C., Beaulieu-Abdelahad D., Mathura V. S., Brem S., Mullan M. 2010. Impaired orthotopic glioma growth and vascularization in transgenic mouse models of Alzheimer's disease. *Journal of Neuroscience.* 30(34): 11251-11258.

Parsons D. W., Jones S., Zhang X., Lin J. C., Leary R. J., Angenendt P., Mankoo P., Carter H., Siu I. M., Gallia G. L., Olivi A., McLendon R., Rasheed B. A., Keir S., Nikolskaya T., Nikolsky Y., Busam D. A., Tekleab H., Diaz L. A. Jr, Hartigan J., Smith D. R., Strausberg R. L., Marie S. K., Shinjo S. M., Yan H., Riggins G. J., Bigner D. D., Karchin R., Papadopoulos N., Parmigiani G., Vogelstein B., Velculescu V. E., Kinzler K. W. 2008. An integrated genomic analysis of human glioblastoma multiforme. *Science (New York. N.Y.).* 321(5897): 1807-1812.

Price R. L., Chiocca E. A. 2014. Evolution of Malignant Glioma Treatment: From Chemotherapy to Vaccines to Viruses. *Neurosurgery.* 61(1): 74-83.

Price S. J., Allinson K., Liu H., Boonzaier N. R., Yan J. L., Lupson V. C., Larkin T. J. 2017. Less Invasive Phenotype Found in Isocitrate Dehydrogenase-mutated Glioblastomas than in Isocitrate Dehydrogenase Wild-Type Glioblastomas: A Diffusion-Tensor Imaging Study. *Radiology.* 283(1): 215-221.

Quistgaard E. M., Madsen P., Groftehauge M. K., Nissen P., Petersen C. M., Thirup S. S. 2009 Ligands bind to Sortilin in the tunnel of a ten-bladed beta-propeller domain. *Nature Structural & Molecular Biology* 16(1): 96–98.

Ray B., Chopra N., Long J. M., Lahiri D. K. 2014. Human Primary Mixed Brain Cultures: Preparation, Differentiation, Characterisation and Application to Neuroscience Research. *Molecular Brain.* 7: 63.

Riedel I. B., Hermans-Borgmeyer I., Hübner C. A. 2002. SorLA, a member of the LDL receptor family, is expressed in the collecting duct of the murine kidney. *Histochemistry and Cell Biology.* 118(3): 183-191.

Rose-John S. 2012. IL-6 Trans-Signaling via the Soluble IL-6 Receptor: Importance for the Pro-Inflammatory Activities of IL-6. *International Journal of Biological Sciences*. 8(9): 1237–1247.

Sakariassen P. Ø., Immervoll H., Chekenya M. 2007. Cancer stem cells as mediators of treatment resistance in brain tumors: status and controversies. *Neoplasia*. 9(11): 882-892.

Salgado I. K., Serrano M., García J. O., Martínez N. A., Maldonado H. M., Báez-Pagán C. A., Lasalde-Dominicci J. A., Silva W. I. 2012. SorLA in Glia: Shared Subcellular Distribution Patterns with Caveolin-1. *Cellular and Molecular Neurobiology*. 32(3): 409–421.

Sánchez-Valle J., Tejero H., Ibáñez K., Portero J. L., Krallinger M., Al-Shahrour F., Tabarés-Seisdedos R., Baudot A., Valencia A. A molecular hypothesis to explain direct and inverse co-morbidities between Alzheimer's Disease, Glioblastoma and Lung cancer. *Scientific Reports.* 7(1): 4474.

Sandoval-Hernández A. G., Buitrago L., Moreno H., Cardona-Gómez G. P., Arboleda G. 2015. Role of Liver X Receptor in AD Pathophysiology. *PLoS One.* 10(12): e0145467.

Schmidt V., Sporbert A., Rohe M., Reimer T., Rehm A., Andersen O. M., Willnow T. E. 2007. SorLA/LR11 Regulates Processing of Amyloid Processing of Amyloid Precursor Protein via Interactions with Adaptors GGA and PACS-1. *The Journal of Biological Chemistry.* 282: 32956-32964.

Schmidt V., Subkhangulova A., Willnow T. E. 2017. Sorting receptor SORLA: cellular mechanisms and implications for disease*. Cellular and Molecular Life Sciences*. 74(8): 1475–1483.

Shi H. B., Tang B., Liu Y. W., Wang X. F., Chen G. J. 2015. Alzheimer disease and cancer risk: a meta-analysis. *Journal of Cancer Research and Clinical Oncology*. 141(3):485-94.

Silva D. F. F., Esteves A. R., Oliveira C. R., Cardoso S. M. 2011. Mitochondria: the common upstream driver of amyloid-β and tau pathology in Alzheimer's disease. *Current Alzheimer Research.* 8: 563-572.

Sugita Y., Ohwada C., Kawaguchi T., Muto T., Tsukamoto S., Takeda Y., Mimura N., Takeuchi M., Sakaida E., Shimizu N., Tanaka H., Abe D., Fukazawa M., Sugawara T., Aotsuka N., Nishiwaki K., Shono K., Ebinuma H., Fujimura K., Bujo H., Yokote K., Nakaseko C. 2016. Prognostic impact of serum soluble LR11 in newly diagnosed diffuse large B-cell lymphoma: A multicenter prospective analysis. *Clinica Chimica Acta; International Journal of Clinical Chemistry.* 463: 47-52.

Takayama K., Tsutsumi S., Suzuki T., *et al.* 2009. Amyloid Precursor Protein Is a Primary Androgen Target Gene That Promotes Prostate Cancer Growth. *Cancer Research.* 69: 137-142.

Tateishi K. and Yamamote T. 2019. IDH-Mutant Gliomas. IDH-Mutant Gliomas [Online First], IntechOpen, DOI: 10.5772/intechopen.84543. Available from: https://www.intechopen.com/online-first/idh-mutant-gliomas.

Terai K., Jiang M., Tokuyama W., Murano T., Takada N., Fujimura K., Ebinuma H., Kishimoto T., Hiruta N., Schneider W. J., Bujo H. 2016. Levels of soluble LR11/SorLA are highly increased in the bile of patients with biliary tract and pancreatic cancers. *Clinica Chimica Acta; International Journal of Clinical Chemistry.* 457: 130-136.

Thonberg H., Chiang H. H., Lilius L., Forsell C., Lindström A. K., Johansson C., Björkströn J., Thordardottir S., Sleegers K., Van Broeckhoven C., Rönnbäck A. Graff C. 2017. Identification and

description of three families with familial Alzheimer disease that segregate variants in the SORL1 gene. *Acta Neuropathologica Communications.* 5(1): 43.

Touat M., Idbaih A., Sanson M., Ligon K. L. 2017. Glioblastoma Targeted Therapy: Updated Approaches from Recent Biological Insights. *Annals of Oncology: Official Journal of the European Society for Medical Oncology.* 28(7): 1457-1472.

Tvedt T. H. A., Ersvaer E., Tveita A. A., Bruserud Ø. 2017. Interleukin-6 in Allogeneic Stem Cell Transplantation: Its Possible Importance for Immunoregulation and As a Therapeutic Target. *Frontiers in Immunology*. 8: 667.

UniProt. (2017). UniProtKB - Q92673 (SORL_HUMAN). Available: http://www.uniprot.org/uniprot/Q92673. Last accessed 12th Sep 2018

Van Meir E., Sawamura Y., Diserens A. C., Hamou M. F., de Tribolet N. 1990. Human glioblastoma cells release interleukin 6 *in vivo* and *in vitro*. *Cancer Research.* 50: 6683–6688.

Venkataramani V., Rossner C., Iffland L. 2010. Histone Deacetylase Inhibitor Valproic Acid Inhibits Cancer Cell Proliferation via Down-regulation of the Alzheimer Amyloid Precursor Protein. *Journal of Biological Chemistry*. 285: 10678-10689.

Vogel T. W., Zhuang Z., Li J., Okamoto H., Furuta M., Lee Y-S., Zeng W., Oldfield E. H., Vortmeyer A. O., Weil R. J. 2017. Proteins and Protein Pattern Differences between Glioma Cell Lines and Glioblastoma Multiforme. *Clinical Cancer Research.* 11(10): 3624-3632.

Wang H., Lathia J. D., Wu Q., Wang J., Li Z., Heddleston J. M., Eyler C. E., Elderbroom J., Gallagher J., Schuschu J., MacSwords J., Cao Y., McLendon R. E., Wang X. F., Hjelmeland A. B., Rich J. N. 2009. Targeting interleukin 6 signaling suppresses glioma stem cell survival and tumor growth. *Stem Cells.* 27(10): 2393-2404.

Willnow T. E., Andersen O. M. 2013. Sorting receptor SORLA – a trafficking path to avoid Alzheimer disease. *Journal of Cell Science* 126: 2751-2760.

Willnow T. E., Petersen C. M., Nykjaer A. 2008. VPS10P-domain receptors - regulators of neuronal viability and function. *Nature Reviews Neuroscience*. 9: 899–909.

Wirsching H.G., Galanis E., Weller M. 2016. Glioblastoma. *Handbook of Clinical Neurology.* 134: 381-397.

Yamamoto M., Ikeda K., Ohshima K., Tsugu H., Kimura H., Tomonaga M. 1997 Increased expression of low density lipoprotein receptor-related protein/alpha2-macroglobulin receptor in human malignant astrocytomas. *Cancer Res.* 57:2799-2805.

Yamazaki H., Bujo H., Kusunoki J. *et al*. 1996. Elements of neural adhesion molecules and a yeast vacuolar protein sorting receptor are present in a novel mammalian low density lipoprotein receptor family member. *Journal of Biological Chemistry.* 271: 24761–24768.

Youn P., Chen Y., Furgeson D.Y. 2015. Cytoprotection against beta-amyloid (A beta) peptide- mediated oxidative damage and autophagy by Keap1 RNAi in human glioma U87mg cells. *Neuroscience Research*. 94: 70-78.

Zhao H., Zhu J., Cui K., Xu X., O'Brien M., Wong K. K., Kesari S., Xia W., Wong S.T. 2009. Bioluminescence imaging reveals inhibition of tumor cell proliferation by Alzheimer's amyloid beta protein. Cancer Cell Int. 9:15.

Zhu Y., Bujo H., Yamazaki H., Ohwaki K., Jiang M., Hirayama S., Kanaki T., Shibasaki M., Takahashi K., Schneider W. J., Saito Y. 2004. LR11, an LDL Receptor Gene Family Member, is a Novel Regulator of Smooth Muscle Cell Migration. *Circulation Research.* 94: 752-758.

Zipfel G. J., Han H., Ford A. L., Lee J-M. Cerebral Amyloid Angiopathy Progressive Disruption of the Neurovascular Unit. *Stroke.* 40(1): S16-S19.

Zollo A., Allen Z., Rasmussen H. F., Iannuzzi F., Shi Y., Larsen A., Maier T. J., Matrone C. 2017. Sortilin-Related Receptor Expression in Human Neural Stem Cells Derived from Alzheimer's Disease Patients Carrying the APOE Epsilon 4 Allele. *Neural Plasticity* 2017:1892612.

CHAPTER 8

APPENDIX

Appendix 1. Haematoxylin solution protocol:

- Heat up 2L dH_2O to boil and then turn off heat.

- Slowly add 200g potassium alum to dissolve in the 2L dH_2O.

- Separately, dissolve 10g haematoxylin in 100ml of ethanol

- The solutions are mixed left for 1 minute before then slowly adding 5g mercuric oxide.

- The solution is to be then rapidly cooled on ice and stored in the dark.

- Prior to use, the required amount of haematoxylin is filtered, with 0.5ml glacial acetic acid per 60ml haematoxylin added. Storage is indefinite.

- The haematoxylin solution can be used up to three times, with it being filtered between each use if the time between exceeds 12hrs.

Appendix 2. Antigen retrieval solution preparation:

- Dissolve 2.88g citric acid (anhydrous) in 1500ml dH_2O.

- Adjust the solution to pH 6.0.

- Add 0.75ml Tween 20.

Appendix 3. Endogenous peroxidase quench solution:

- Depending upon the volume required, add the equivalent to 0.3% of the amount of

  methanol used of 30% (w/v) hydrogen peroxide.

Appendix 4. Seeding ratio for cell lines from confluent T75 flask to coverslips on 12-well plates for IF

- SVGp12 = 1:20

- U87MG = 1:30

- T98G = 1:30

Appendix 5. Murine xenograft animal qualitative data (A), cell count significance between tumour and non-tumour region (B), and cell density data (C). Cell counts between all the tumour and non-tumour regions show a significant difference ($p \leq 0.05$). FOV=3, n=3.

A

| Brain Designation	Surgery Date	Cull Date	Days Passed	Reason for Cull
#39	25/10/2017	20/11/2017	26	Weight Loss
3101C2	23/05/2017	17/06/2017	25	Weight Loss, Lack of Movement
3101C6	25/05/2017	22/06/2017	28	Weight Loss, Lack of Movement, Pale

B

Paired Samples Test

|		Paired Differences			95% Confidence Interval of the Difference				
		Mean	Std. Deviation	Std. Error Mean	Lower	Upper	t	df	Sig. (2-tailed)
Pair 1	#39 Tumour Cell Count - #39 Non-Tumour Cell Count	398.22222	115.16671	66.49153	112.13226	684.31218	5.989	2	.027
Pair 2	3101C2 Tumour Cell Count - 3101C2 Non-Tumour Cell Count	467.66667	25.91225	14.96044	403.29708	532.03625	31.260	2	.001
Pair 3	3101C6 Tumour Cell Count - 3101C6 Non-Tumour Cell Count	447.88889	54.28457	31.34121	313.03854	582.73924	14.291	2	.005

C

| Brain Designation	Non-Tumour Area (µm2)	Average Non-Tumour Cell Count	Cell Density (per µm2)
#39	295553.97	68,672	0.232349596
3101C2	31029.083	6,573.65	0.211854449
3101C6	255724.454	52,248	0.204314749
Brain Designation	Tumour Area (µm2)	Average Tumour Cell Count	Cell Density (per µm2)
#39	227827.544	139,646	0.612944177
3101C2	44448.616	29,283.61	0.658819448
3101C6	220039.235	139,148	0.632377427

Appendix 6. Montage composites of SorLA and haematoxylin stained non-tumour and tumour image replicates used for analysis. #39 SorLA & Haematoxylin non-tumour tissue replicates being rows A-C and tumour tissue being rows D-F. 3101C2 SorLA & Haematoxylin non-tumour are G-I and tumour being J-L. 3101C6 SorLA & Haematoxylin non-tumour are M-O and tumour being P-R.
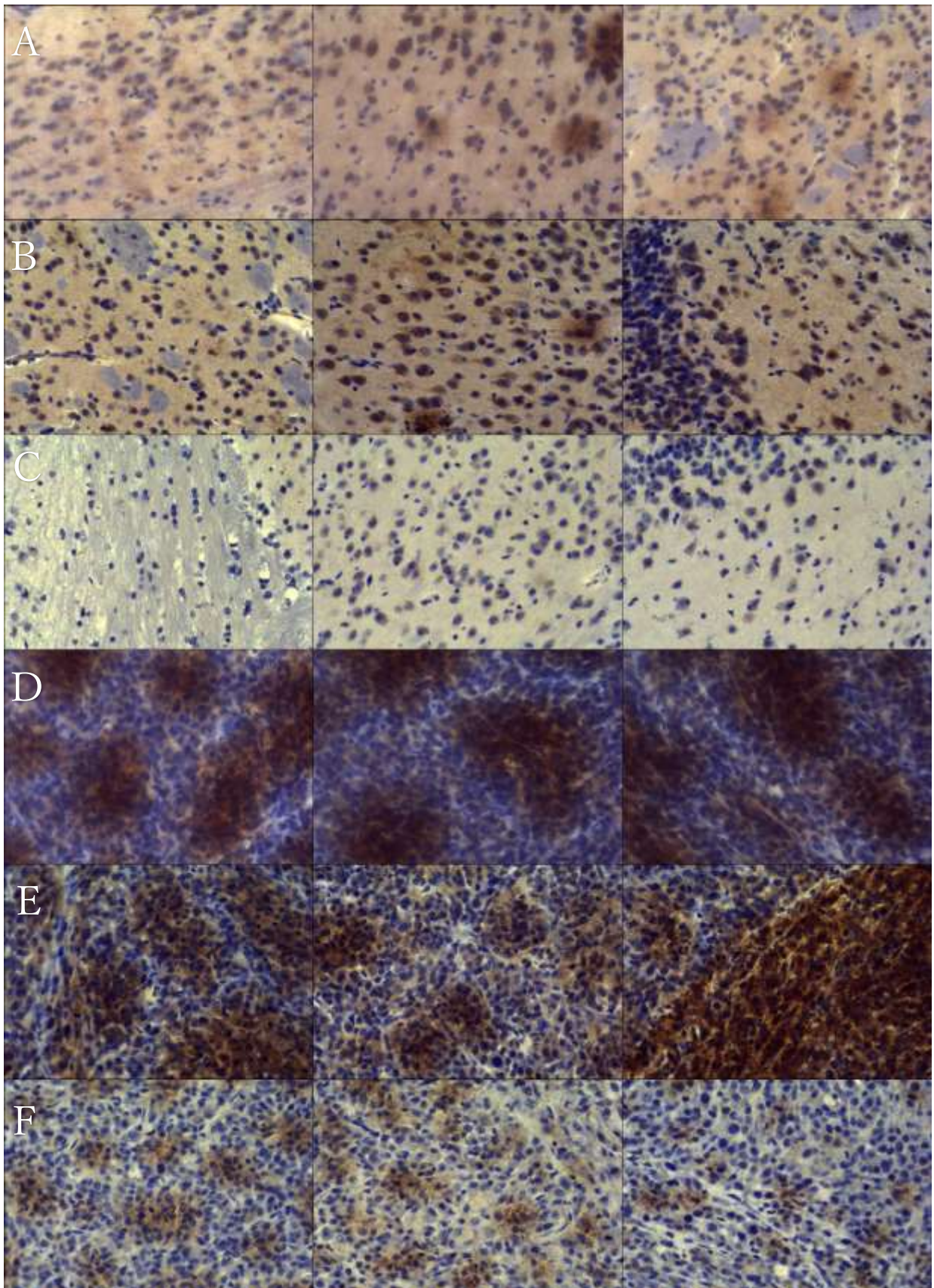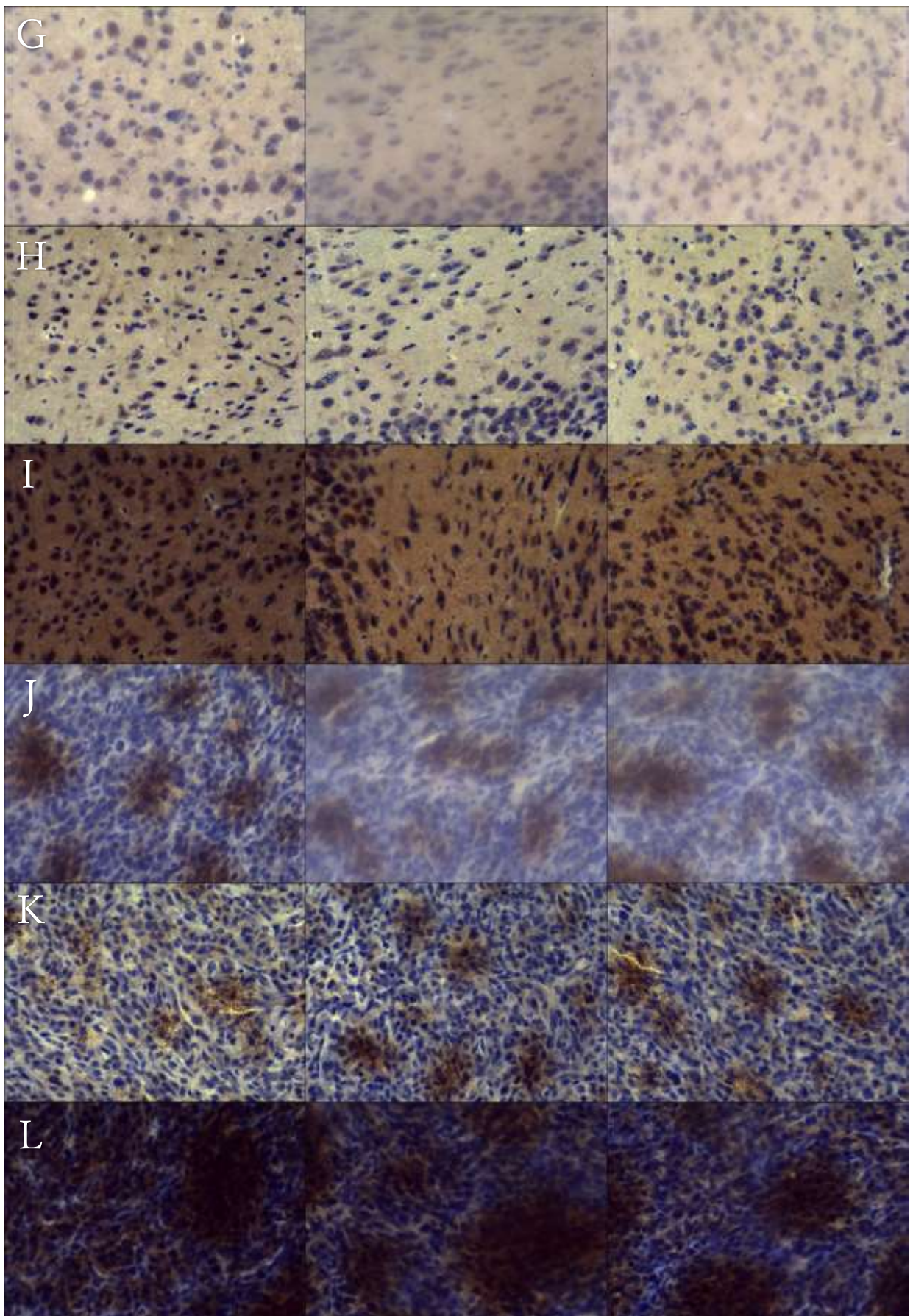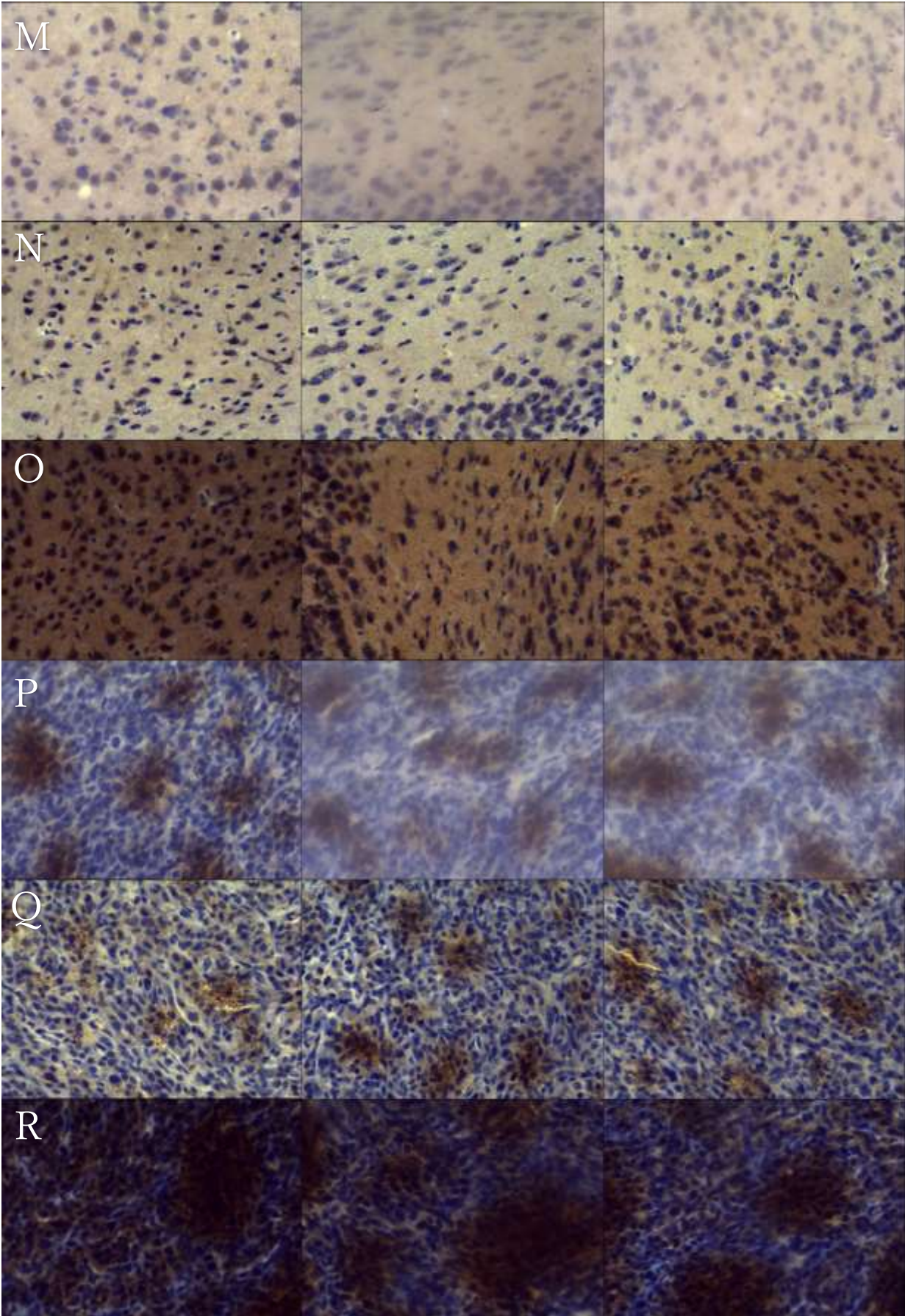
Appendix 7. Montage composites of amyloid beta and haematoxylin stained non-tumour and tumour image replicates used for analysis. #39 Amyloid beta and haematoxylin non-tumour tissue replicates being rows A-C and tumour tissue being rows D-F. 3101C2 Amyloid beta and haematoxylin non-tumour are G-I and tumour being J-L. 3101C6 Amyloid beta and haematoxylin non-tumour are M-O and tumour being P-R.
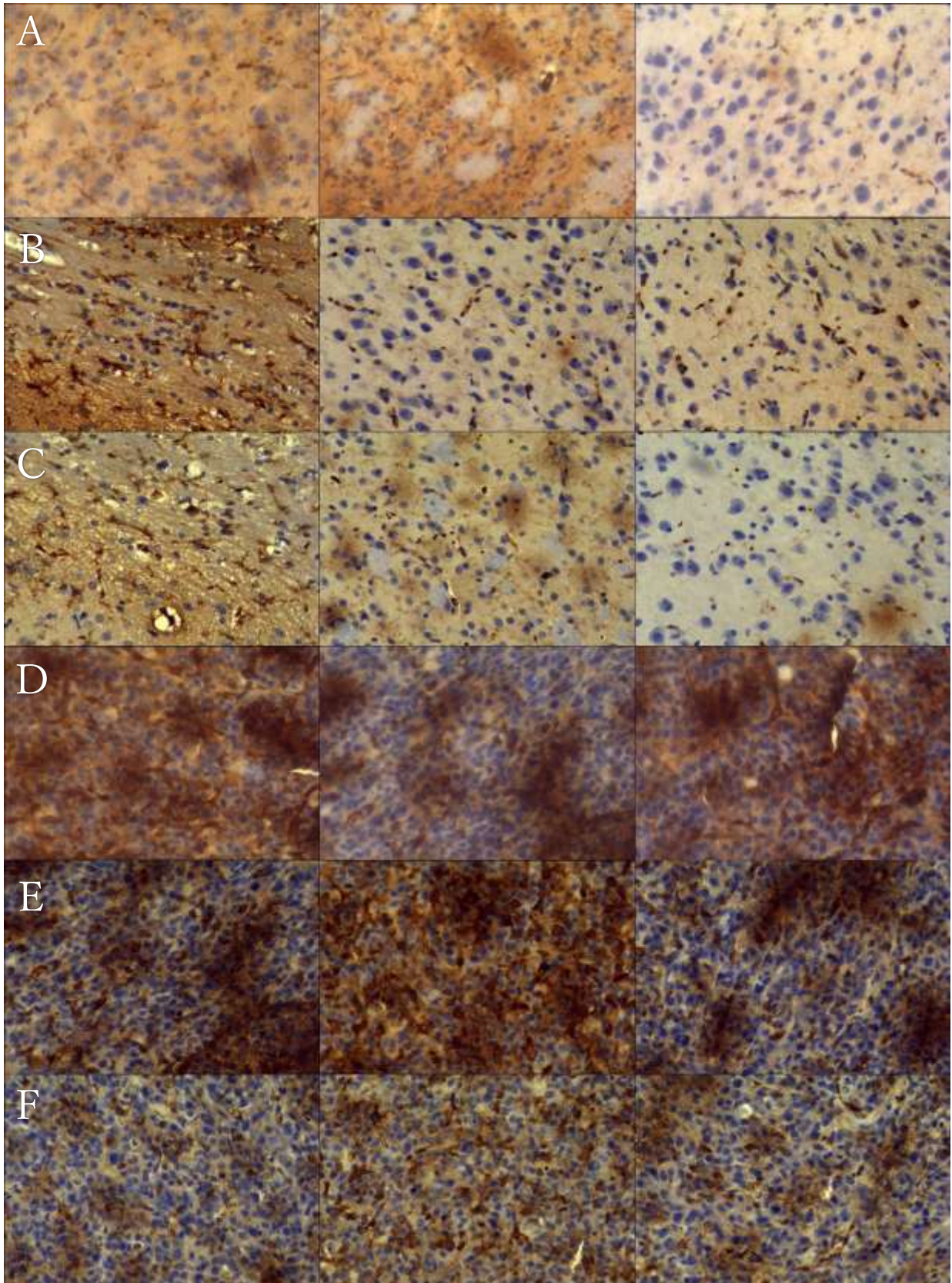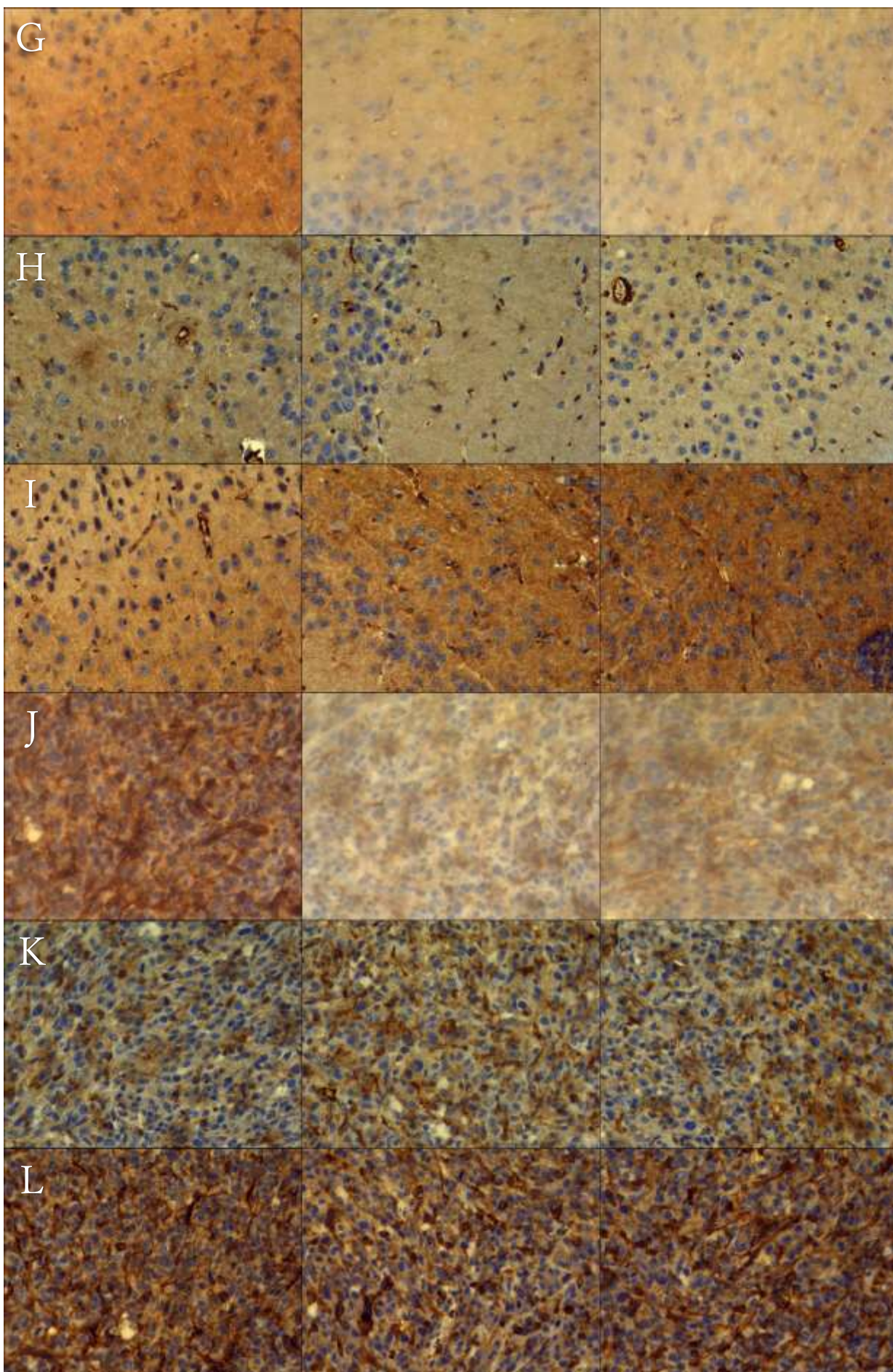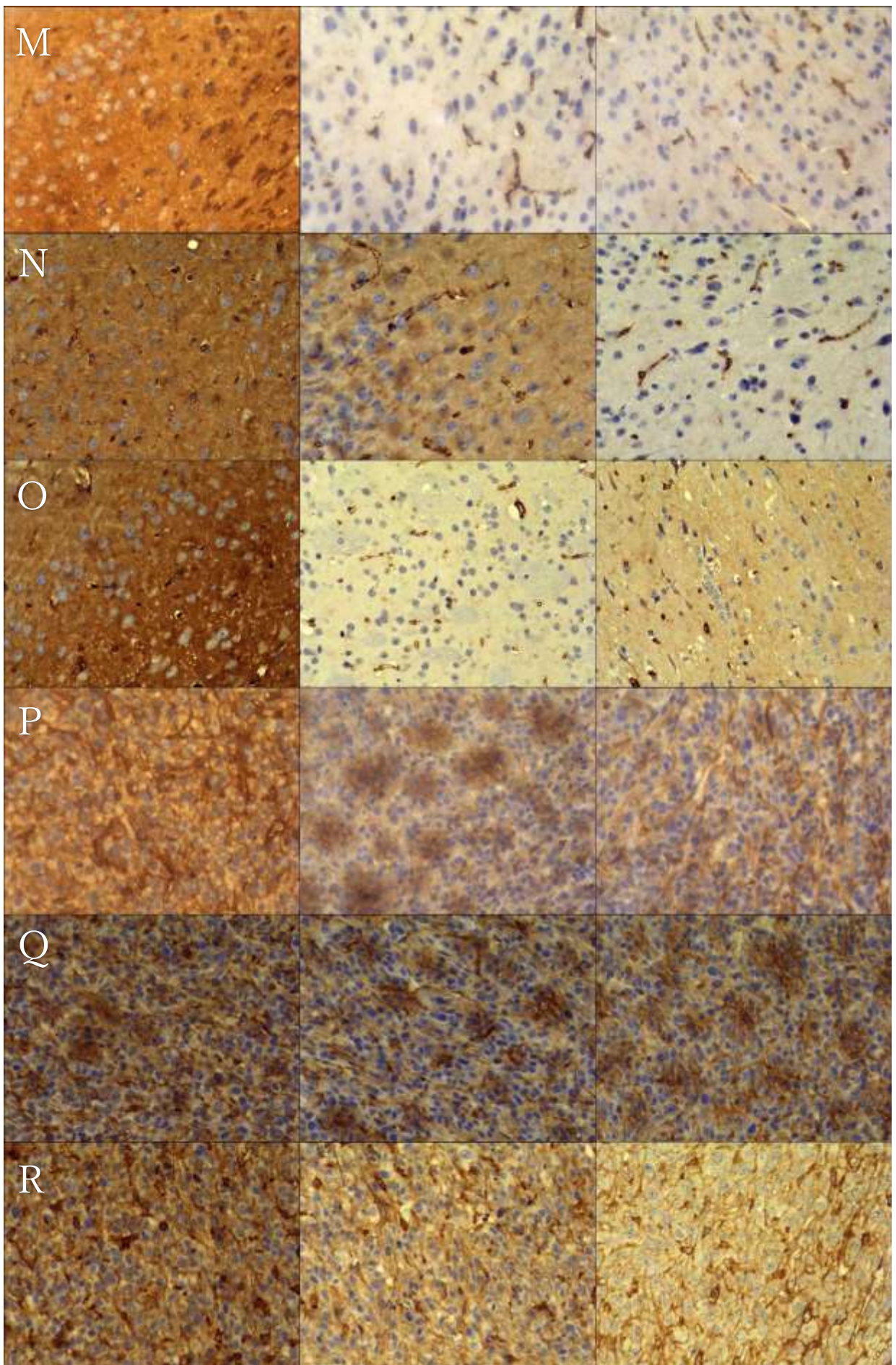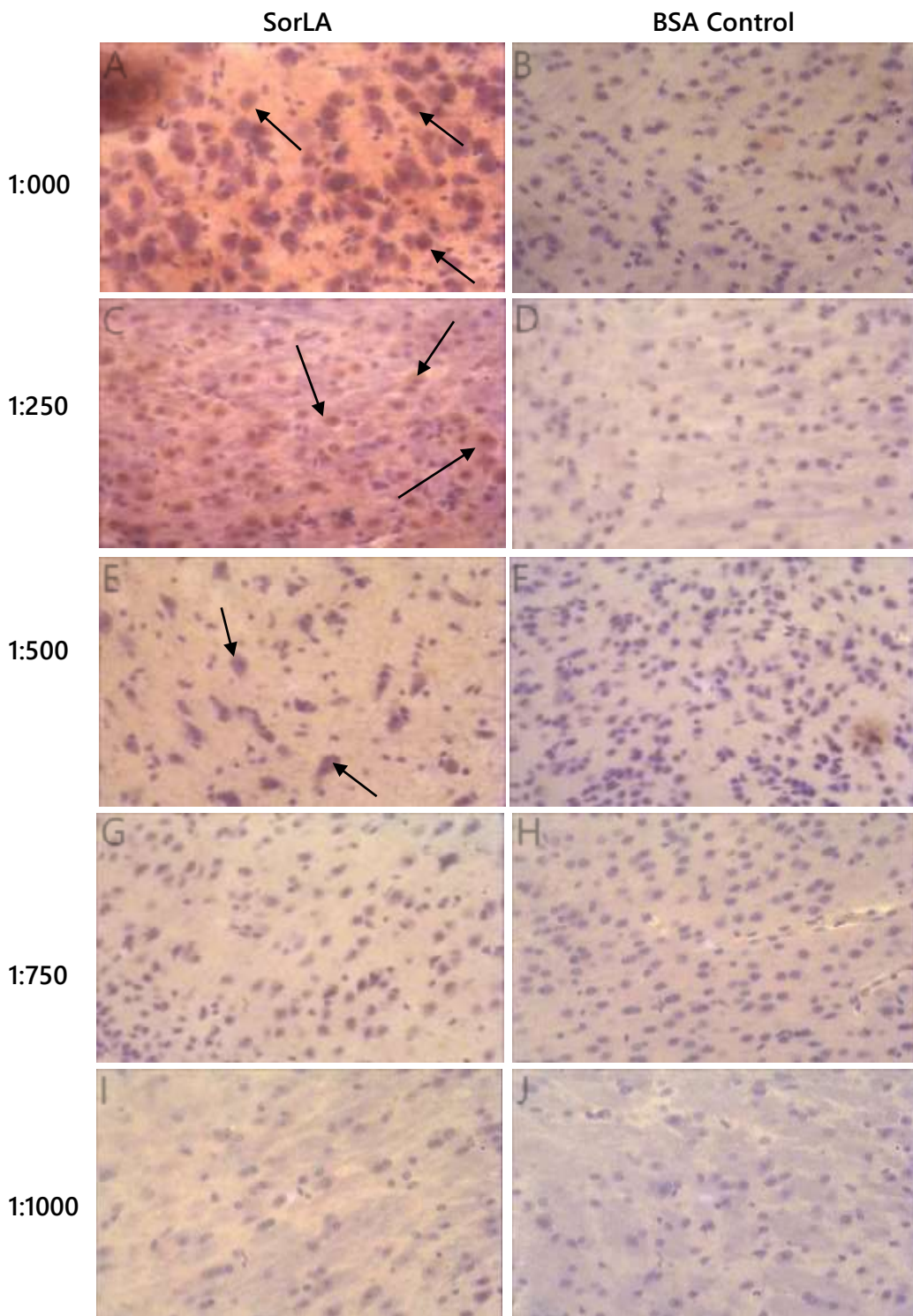
Appendix 8. Tabulated data on IF fluorescence.

|	Mean	Std. Deviation	Standard Error Mean
SVG	14.711	5.418	2.423
U87MG	22.562	17.462	7.809
T98G	23.538	30.69	13.725
NHA	36.733	33.322	14.337

Appendix 9. Optimisation of the anti-SorLA antibody on non-tumour tissue sections.

Concentration dependent immunoreactivity was detected in sections exposed to anti-SorLA antibody (black arrows). Sections where primary antibody had been omitted lacked immunoreactivity, with only the haematoxylin being taken up (blue/purple nuclei). Mag x40. Scale bar, 5µm, n=3.

Appendix 10. Optimisation of the anti-Aβ antibody on tumour tissue sections.

	Amyloid-β	BSA
1:500		
1:750		
1:1000		
1:2000		
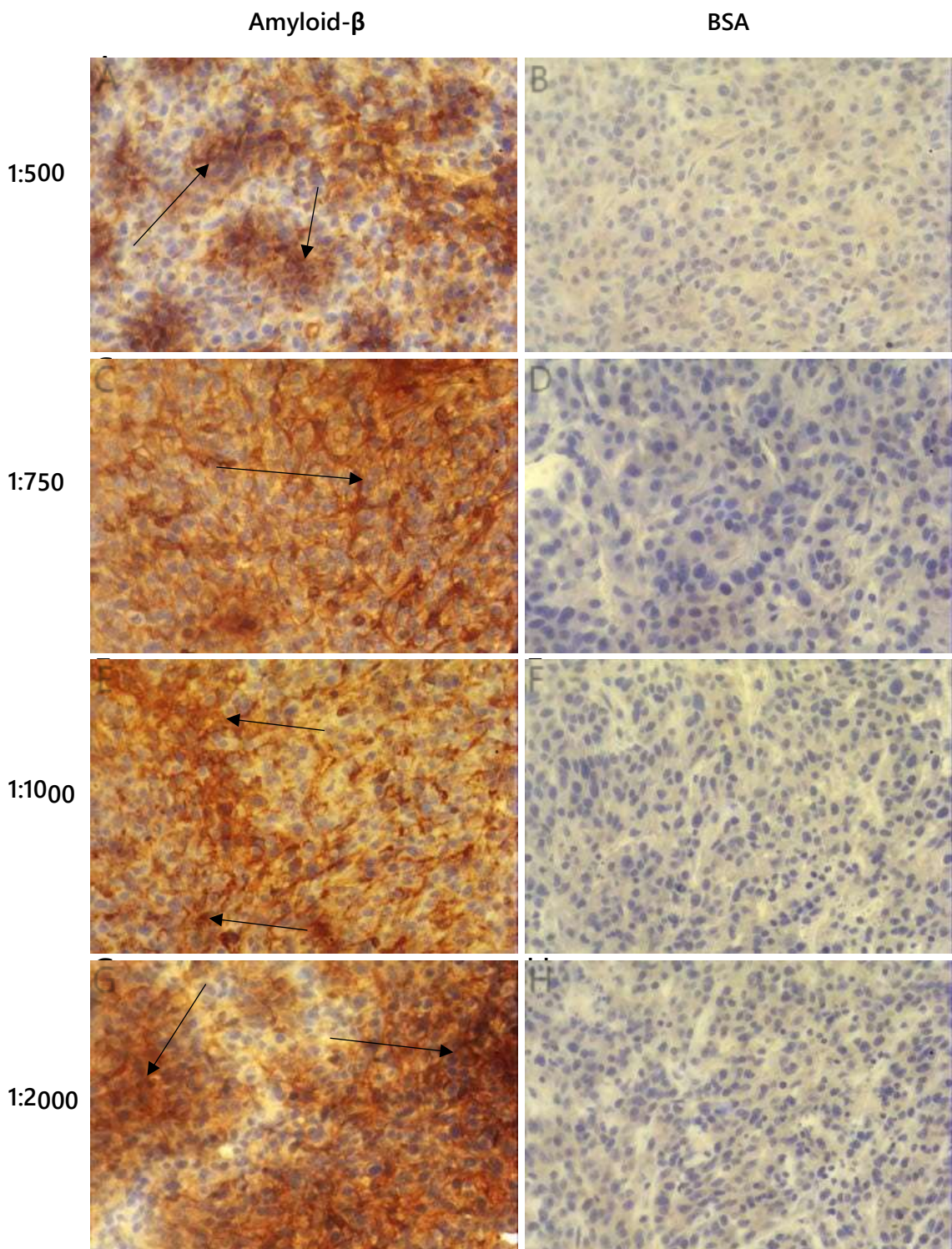
Aβ expression was detected as brown DAB staining within the tumour as Aβ plaques (black arrows). BSA control shows no DAB immunoreactivity with only the haematoxylin counterstain being taken up (blue/purple nuclei). The final concentration chosen to use was 1:500. Scale bar 5μm. n=3. Mag x40.

Appendix 11. Validation of immunohistochemical labelling of murine xenograft brain.
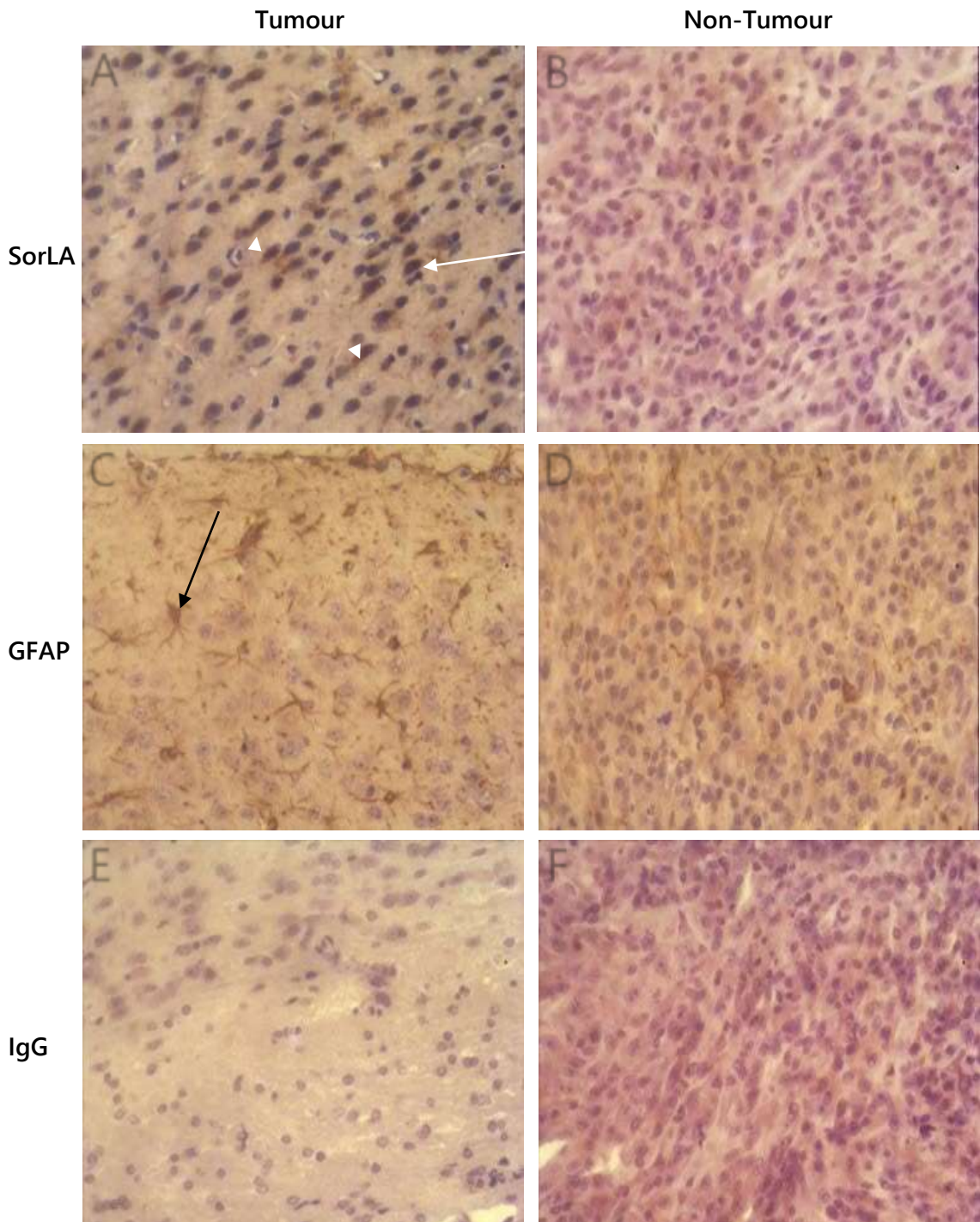
	Tumour	Non-Tumour

A degree of intracellular SorLA was observable in the non-tumour (A) (white arrows), with little immunoreactivity within the tumour (B). GFAP expression was detected in the non- tumour region (C) (black arrow) and reduced expression detected within the tumour (D). The negative isotype (IgG) control for non-specific binding showed minimal binding within both non-tumour and tumour regions (E, F). Scale bar 5μm. FOV=3, n=3. Mag x40.

Appendix 12. Tabulated data on SorLA intensity and average area of SorLA deposits.

	Mean	Std. Deviation	Std. Error Mean	t	Degrees of Freedom	Significance	α
#39	95.02	33.94	7.999	-2.065	8	0.073	0.05
3101C2	78.1	27.95	6.587	0.348	8	0.737	0.05
3101C6	94.84	47.01	11.081	-1.688	8	0.13	0.05
Normalised	89.318	37.324	5.079133311	-2.379	26	0.025	0.05

	Mean	Std. Deviation	Std. Error Mean	t	Degrees of Freedom	Significance	α
#39	160.6	60.93	20.31	7.906	8	<0.001	0.05
3101C2	40.06	14.89	4.964	8.069	8	<0.001	0.05
3101C6	66.26	37.49	12.5	5.303	8	<0.001	0.05

**Appendix 13. Tabulated data on amyloid beta intensity and average area of amyloid beta plaques.**

Paired Samples Test

		Paired Differences							
					95% Confidence Interval of the Difference				
		Mean	Std. Deviation	Std. Error Mean	Lower	Upper	t	df	Sig. (2-tailed)
Pair 1	#39 Tumour Intensity - #39 Non-Tumour Intensity	-6.92233	11.62473	4.74578	-19.12174	5.27707	-1.459	5	.204
Pair 2	3101C6 Tumour Intensity - 3101C6 Non-Tumour Intensity	19.67667	22.23459	9.07723	-3.65711	43.01044	2.168	5	.082
Pair 3	3101C2 Tumour Intensity - 3101C2 Non-Tumour Intensity	-24.55417	19.55535	7.98344	-45.07625	-4.03208	-3.076	5	.028

Paired Samples Test

|		Paired Differences							
					95% Confidence Interval of the Difference				
		Mean	Std. Deviation	Std. Error Mean	Lower	Upper	t	df	Sig. (2-tailed)
Pair 1	#39 Tumour Area - #39 Non-Tumour Area	90.60500	76.73258	31.32594	10.07910	171.13090	2.892	5	.034
Pair 2	3101C6 Tumour Area - 3101C6 Non-Tumour Area	91.85517	75.69909	30.90402	12.41385	171.29649	2.972	5	.031
Pair 3	3101C2 Tumour Area - 3101C2 Non-Tumour Area	200.59117	188.78033	77.06925	2.47836	398.70397	2.603	5	.048

Appendix 14. Montage composite of replicate IF-stained cells used in intensity analysis.
U87MG control and SorLA replicates (A), followed by T98G control and SorLA (B), SVGp12 control
and SorLA (C), ending with NHA control and SorLA replicates (D). Scale bar 20µm x40 'oil' mag.
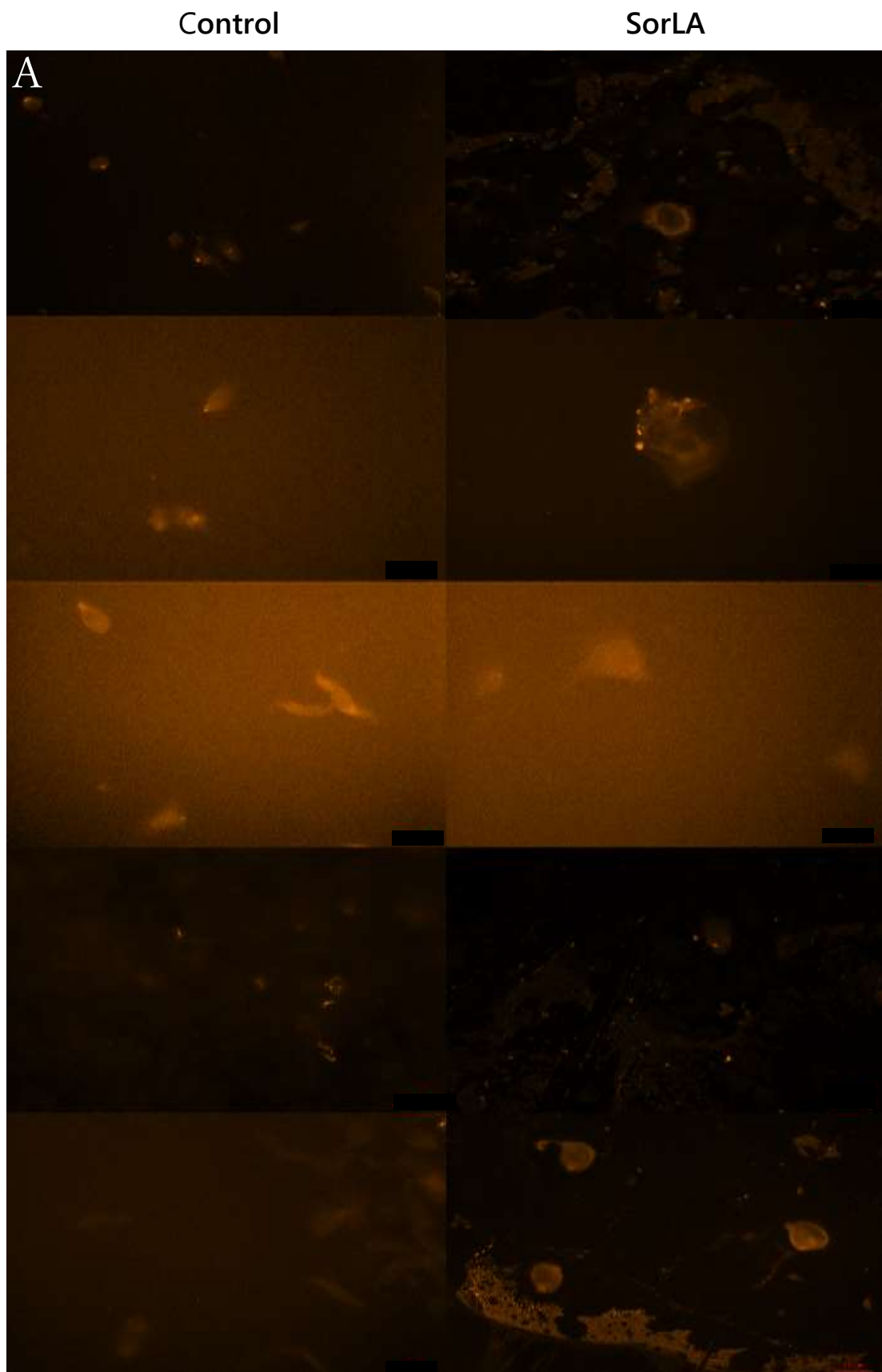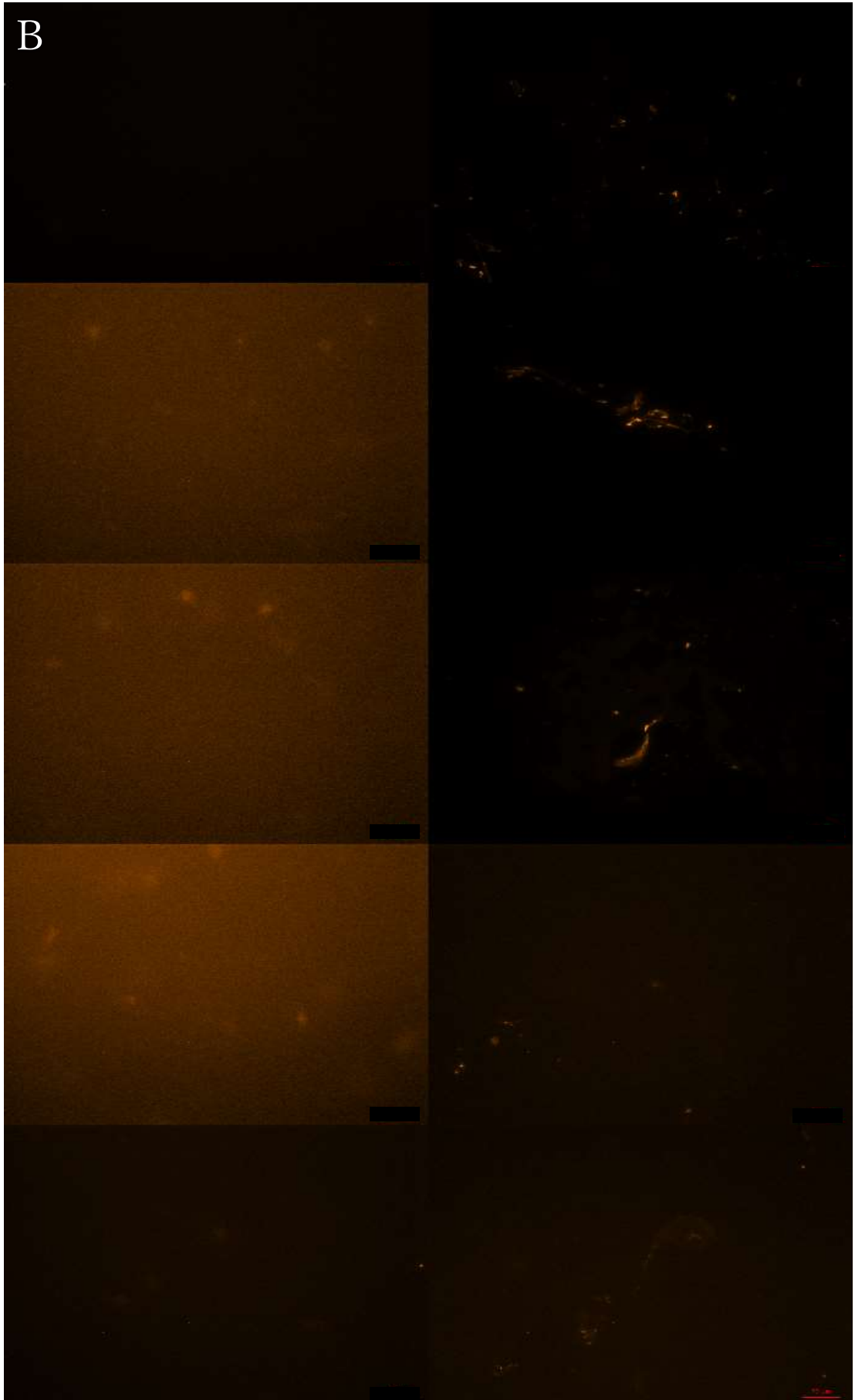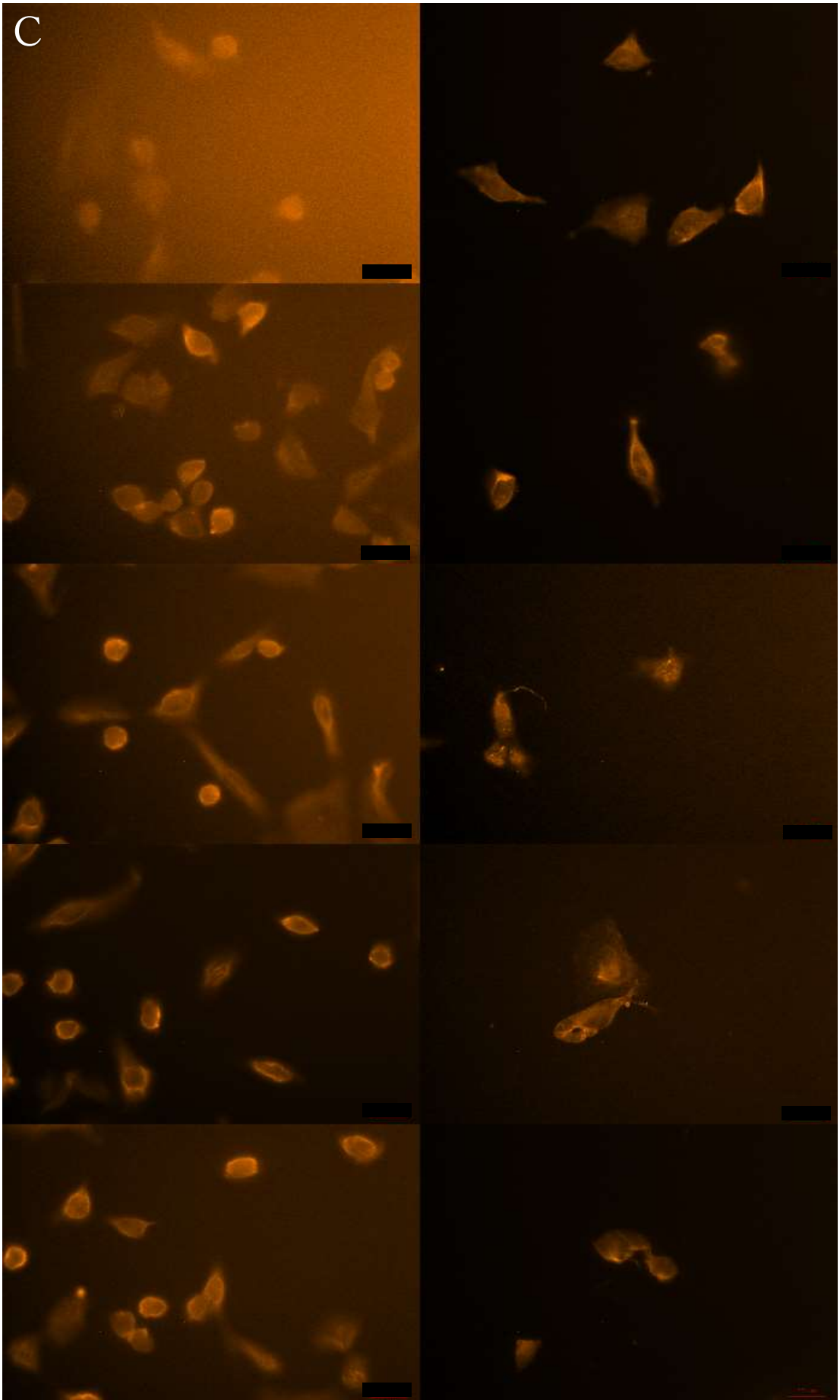
Control   SorLA

Control   SorLA

B

Control   SorLA

C

Control   SorLA